New insights into the geology and mineral potential of the Coast Belt in southwestern Yukon

Steve Israel[1], Don Murphy, Venessa Bennett
Yukon Geological Survey

Jim Mortensen
University of British Columbia, Vancouver BC

Jim Crowley
Boise State University, Boise, Idaho

Israel, S., Murphy, D., Bennett, V., Mortensen, J. and Crowley, J., 2011. New insights into the geology and mineral potential of the Coast Belt in southwestern Yukon. *In:* Yukon Exploration and Geology 2010, K.E. MacFarlane, L.H. Weston and C. Relf (eds.), Yukon Geological Survey, p. 101-123.

ABSTRACT

The southwestern Yukon Coast Belt mapping project is a joint Yukon Geological Survey/Geological Survey of Canada initiative operated under Natural Resources Canada's GEM (Geomapping for Energy and Minerals) program. This project is aimed at investigating the geological relationships and mineral potential of the Kluane Schist, the Ruby Range batholith and the Yukon-Tanana terrane in southwestern Yukon. Bedrock mapping at 1:50 000-scale followed a 400 m line-spaced aeromagnetic survey flown in the winter of 2010. Preliminary results indicate the presence of a northeast-dipping structural stack through an ~40 km-thick crustal section, whereby the Kluane Schist occupies the lowest structural level and the Yukon-Tanana terrane the highest. The Ruby Range batholith intruded along the contact between the Kluane Schist and the Yukon-Tanana terrane, and was emplaced late in the deformation history. An orthogneiss/paragneiss unit of unknown tectonic affinity was mapped structurally between the Ruby Range and the Kluane Schist. Detrital zircon analyses from two samples of Kluane Schist indicate that the onset of deposition for this metasedimentary sequence occurred after *ca.* 94 Ma. Two significant metamorphic events, dated at 82 and 70 Ma, affected the Kluane Schist. This indicates that original structural juxtaposition between the Kluane Schist and the Yukon-Tanana terrane pre-dated intrusion of the Ruby Range batholith.

Mineral potential in the Coast Belt area is significant and includes porphyry Cu-Mo-Au, epithermal Au-Ag and orogenic Au occurrences. The upper level of the Ruby Range batholith is most prospective for porphyry and epithermal mineralization, while the Kluane Schist is most prospective for orogenic Au mineralization.

[1]*steve.israel@gov.yk.ca*

INTRODUCTION

The southwestern Yukon Coast Belt (SYCB) mapping project is a joint Yukon Geological Survey/Geological Survey of Canada initiative operated under Natural Resources of Canada's GEM (Geomapping for Energy and Minerals) program. The mapping project is one of several that comprise the Edges Project. The study area is located in southwest Yukon and extends from the eastern edge of Kluane Lake, north to Rhyolite Creek, east to Aishihik Lake, and south to the Alaska Highway; it encompasses part of the Kluane Lake and Aishihik 1:250 000-scale map area (NTS 115G and 115H, respectively; Fig. 1). Access is mainly by helicopter but the boundaries of the area can be accessed along the Aishihik road in the east, the Cultus Bay road in the west and the Alaska Highway in the south. Much of the area is contained within the Ruby and Nisling ranges that consist of rugged to rounded mountains reaching elevations of up to 2200 m, and separated by large valleys filled with Quaternary deposits. The mountains become less rugged and lower in elevation to the north. Vegetation is limited to scrub grass at higher elevations with open spruce forests occupying areas below ~1200 m and swampy wetlands in the lowest and widest valleys.

Figure 1. *Location of the Coast Belt project area.*

Bedrock mapping activities were based out of a camp near Silver City and took place over a six week period in June and July 2010. Mapping followed up on a 400 m line-spacing aeromagnetic survey acquired in February and March 2010 (Kiss, 2010) and covering approximately eleven 1:50 000-scale map sheets.

The main goals of the project were to investigate the geological relationships and mineral potential of the Kluane Schist, the Ruby Range batholith and the Yukon-Tanana terrane in southwest Yukon. This paper summarizes bedrock geology data collected during the summer 2010 and presents preliminary results of detrital and igneous zircon analyses from the Kluane Schist and Ruby Range batholith. Key results from this study include:

1. The structural stacking of the tectonic elements creates an exposed section of crust roughly 40 km thick. This section includes an entire batholith from its roots up into the porphyry and epithermal realms, and its overlying volcanic carapace.
2. The Ruby Range batholith is syn-to-post tectonic and becomes more felsic higher in the crustal section.
3. A unit of orthogneiss/paragneiss of uncertain age and correlation occurs along the base of the batholith and structurally above the Kluane Schist.
4. The potential for porphyry and epithermal style mineralization increases up crustal section.
5. The depositional age of the Kluane Schist is constrained by detrital zircons as young as ~95 Ma. The provenance of the Kluane Schist is likely an uplifted Yukon-Tanana terrane and Jurassic to Cretaceous plutons of the Aishihik batholith and the Coast plutonic complex.
6. LA-ICPMS dating of metamorphic rims on Kluane Schist detrital zircons suggest that metamorphism significantly intense enough to cause Pb loss and new zircon growth occurred at ~82 Ma and ~70 Ma.
7. The lithotectonic relationships observed in southwestern Yukon are similar to those in southeastern Alaska, increasing the potential for orogenic-style gold mineralization.

REGIONAL GEOLOGY AND PREVIOUS WORK

The area north of the Denali fault and southeast of the White River in southwestern Yukon is underlain by three main tectonic elements: 1) the Kluane Schist; 2) the Ruby Range batholith; and 3) the Yukon-Tanana terrane. They form a northeast-dipping structural stack that exposes a roughly 40 km-thick section of crust (Fig. 2). This tectonic

configuration continues to the southeast where the Kluane Schist is structurally truncated by an ambiguous fault zone between the Kluane Schist and the Dezadeash Formation, south of the town of Haines Junction. To the southwest, the Kluane Schist is in fault contact with metasedimentary rocks of the Dezadeash Formation and an enigmatic package of highly deformed and metamorphosed mafic volcanic rocks, informally known as the Bear Creek metavolcanic assemblage. To the northwest, the Kluane Schist and the Ruby Range batholith are cut off by the Denali fault. North of the map area, the Yukon-Tanana terrane is extensively intruded by the Early Jurassic Aishihik and mid-Cretaceous Dawson Range batholiths.

Previous geologic studies in the area were either reconnaissance in nature or focussed on specific tectonic elements. The present study is the first to conduct comprehensive bedrock mapping of the entire area at 1:50,000-scale. Previous 1:250 000-scale bedrock mapping by the Geological Survey of Canada was completed by Muller (1967) in the Kluane Lake map sheet (115G) and by Tempelman-Kluit (1974) in the Aishihik map sheet (115H). More detailed, 1:50 000-scale mapping by Johnston and Timmerman (1994) covered map sheets 115H/6-7. Murphy (2007) and Murphy *et al.* (2008; 2009) completed comprehensive 1:50 000-scale mapping of the area northwest of the current study. Their efforts were concentrated on deciphering the tectonic relationships between the Windy-McKinley terrane, mid- to Late Cretaceous igneous rocks and the Yukon-Tanana terrane. Several metamorphic studies have been carried out within the Yukon-Tanana terrane (Aishihik metamorphic complex) and the Kluane Schist (Erdmer, 1991; Johnston and Erdmer, 1995a; Mezger *et al.*, 2001a), as well as larger-scale tectonic analyses (Erdmer and Mortensen, 1993; Mezger *et al.*, 2001b; Johnston and Canil, 2006).

GEOLOGY OF THE STUDY AREA

The Kluane Schist occupies the lowest exposed structural level in the study area, while the Yukon-Tanana terrane occurs at the highest structural level. The Ruby Range batholith intrudes between and across the other two tectonic elements, obscuring the nature of the contact between them. Younger, more felsic and porphyritic phases of intrusive material outcrop at the top of the batholith, where they are interpreted to be the feeders to intermediate to felsic volcanic rocks that unconformably overly the Yukon-Tanana terrane. These intrusive and volcanic rocks have been informally named here the Rhyolite Creek volcano-plutonic complex (Fig. 3).

YUKON-TANANA TERRANE

Rocks in the northern portion of the project area were previously referred to as the Aishihik Lake metamorphic belt (Tempelman-Kluit, 1974), the Nisling terrane (Wheeler and McFeely, 1991) and the Aishihik metamorphic suite (Erdmer, 1991). Murphy *et al.* (2008) correlated similar rocks along strike to the northwest with the Snowcap and Finlayson assemblages of the Yukon-Tanana terrane. Although the rocks in the SYCB project area are more strongly metamorphosed than those described by Murphy *et al.* (2008), we believe that they are part of the Snowcap and Finlayson assemblages.

The Yukon-Tanana terrane in the project area structurally overlies the Ruby Range batholith and locally occurs as isolated roof pendants. The terrane consists of psammitic schist, quartzite, marble, garnet amphibolite and rare metaplutonic rocks. In the western half of the project area, schist and quartzite are variably carbonaceous, and interlayered with at least two similar beige-weathering carbonate units. Overlying the schists and quartzite are amphibolite units that locally contain abundant garnet up to 4 cm across (Fig. 4). In the eastern half of the project area Yukon-Tanana terrane rocks take on a higher degree of metamorphism, possibly lying within the dynamothermal aureole of the Early Jurassic Aishihik batholith (Johnston and Erdmer, 1995a). Yukon-Tanana terrane in this area comprises quartz-muscovite-garnet schist interlayered with carbonaceous quartzite, garnet amphibolite and thick (up to 75 m), beige to white-weathering marble units. Rare metaplutonic rocks are found interfoliated with the schists. These metaplutonic rocks are generally fine to medium-grained and quartz-diorite to diorite in composition. The structurally highest rocks in Yukon-Tanana terrane consist of coarse-grained, quartz-rich 'grits' and grey weathering carbonaceous quartzite (Fig. 5); the nature of the contact between these and underlying rocks is not known.

The age of the Yukon-Tanana terrane in the project area is not well constrained. Ages of 351 to 343 Ma are reported for meta-igneous rocks in the area by Johnston *et al.* (1996). This provides a lower age constraint for the unit. Elsewhere in the Yukon-Tanana terrane, similar ages are characteristic of metaplutonic rocks of the Simpson Range suite that intrudes the Snowcap assemblage, and overlying metavolcanic rocks of the Finlayson assemblage (Colpron *et al.*, 2006; Murphy *et al.*, 2006).

a

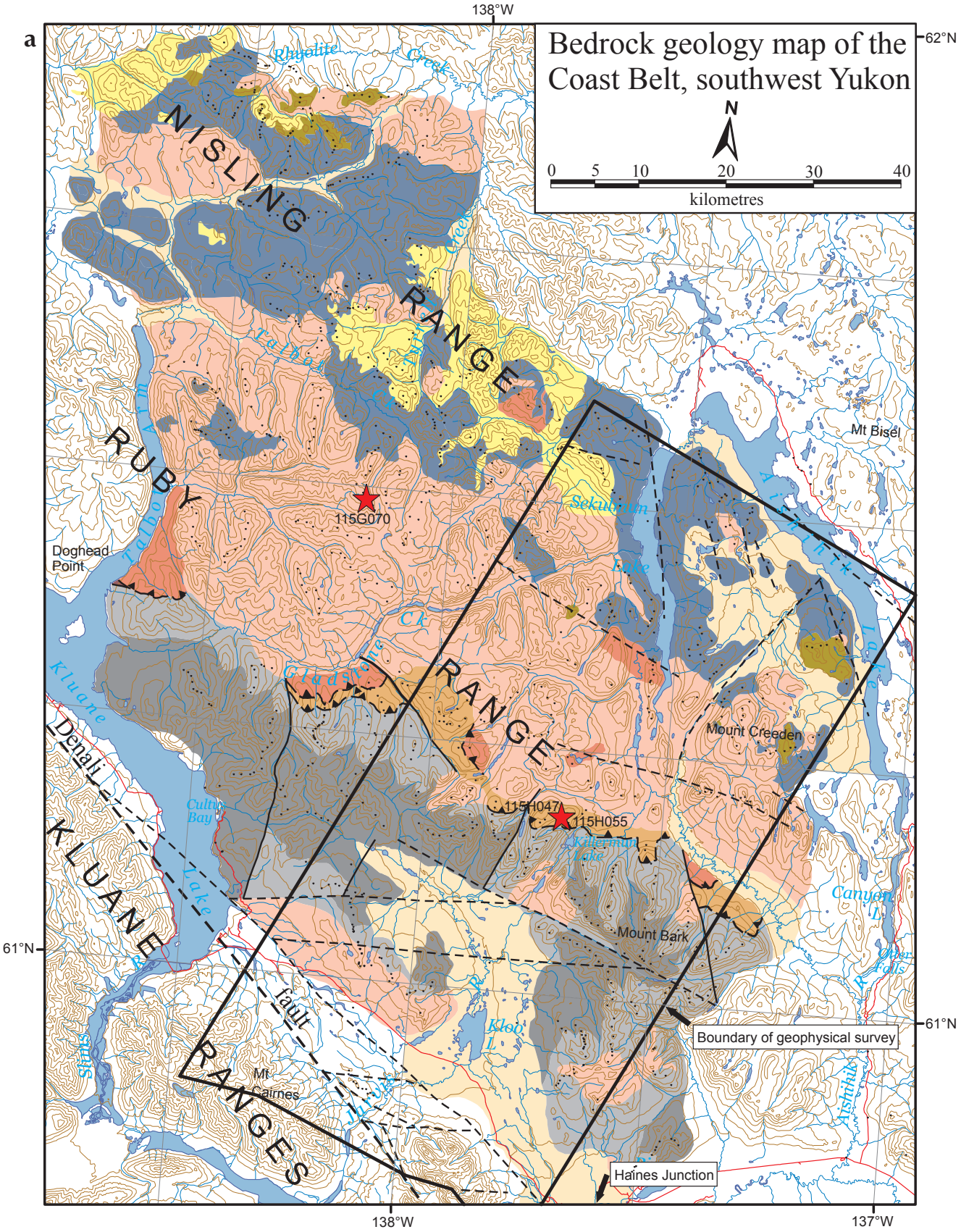
Bedrock geology map of the Coast Belt, southwest Yukon
N
0 5 10 20 30 40
kilometres
138°W
62°N
61°N
137°W
NISLING RANGE
RUBY RANGES
KLUANE RANGES
115G070
115H047
115H055
Doghead Point
Mount Creeden
Mount Bark
Mt Bisel
Haines Junction
Boundary of geophysical survey
Rhyolite Creek
Talbood Creek
Sekulmun Lake
Gladstone Ck
Kluane Lake
Denali fault
Mt Cairnes
Kloo L.
Canyon L.
Otter Falls
Aishihik R.
Aishihik Lake
Jarvis R.
Slims R.
Cultus Bay

b

Lithology

Rhyolite Creek volcanoplutonic complex

light grey, brown and green, intermediate to felsic volcanic rocks; flow banding is common; local volcanic breccia; rare pillows and mafic volcanic rocks

light grey to purple, quartz, feldspar porphyry; quartz is often smokey grey in colour; occurs as thin dykes to large intrusive bodies; intrusive equivalents to intermediate to felsic volcanic rocks

Ruby Range batholith

fine to coarse-grained, salt and pepper, hornblende ± biotite, quartz diorite, rare garnets; medium-grained, light grey to pinkish biotite ± hornblende granodiorite; fine to medium-grained, beige to grey tonalite with distinctive smokey grey quartz; pinkish/grey, biotite granite

strongly to moderately deformed equivalents of undeformed Ruby Range batholith; often has 'gneissic' texture near the base of the batholith

Kluane Schist

dark grey to dark green, strongly deformed and altered ultramafic lenses; light grey, fine-grained talc-schist

light to dark grey, fine-grained, quartz, muscovite schist; variably carbonaceous (more carbonaceous in the northwest of map area); rare light grey carbonate lenses;

dark grey to black, fine-grained, quartz, biotite schist; occasional garnets and plagioclase porphyroblasts; layer parallel, boudinaged quartz veins ubiquitous

Gneiss

beige, orange to grey black, medium- to coarse-grained orthogneiss and paragneiss; mafic layers composed primarily of biotite ± hornblende, leucocratic layers consist of quartz, potassium feldspar and plagioclase; abundant garnet; could be part of Yukon-Tanana terrane or the Kluane Schist

Yukon-Tanana terrane

beige- to brown-weathering quartz, muscovite ± garnet, psammitic schist; dark grey to black carbonaceous biotite ± garnet schist and quartzite; dark green to black garnet amphibolite; grey to cream marble; rare metaplutonic rocks

Symbology

.....fault, geophysically interpreted

.....fault, approximate

.....thrust fault, approximate

.....station locaton

.....road

Figure 2. ***(a)*** *Generalized bedrock geology map of the Coast Belt project area, southwestern Yukon. Red star indicates location of Yukon MINFILE occurrences (2009);* ***(b)*** *legend for bedrock map.*

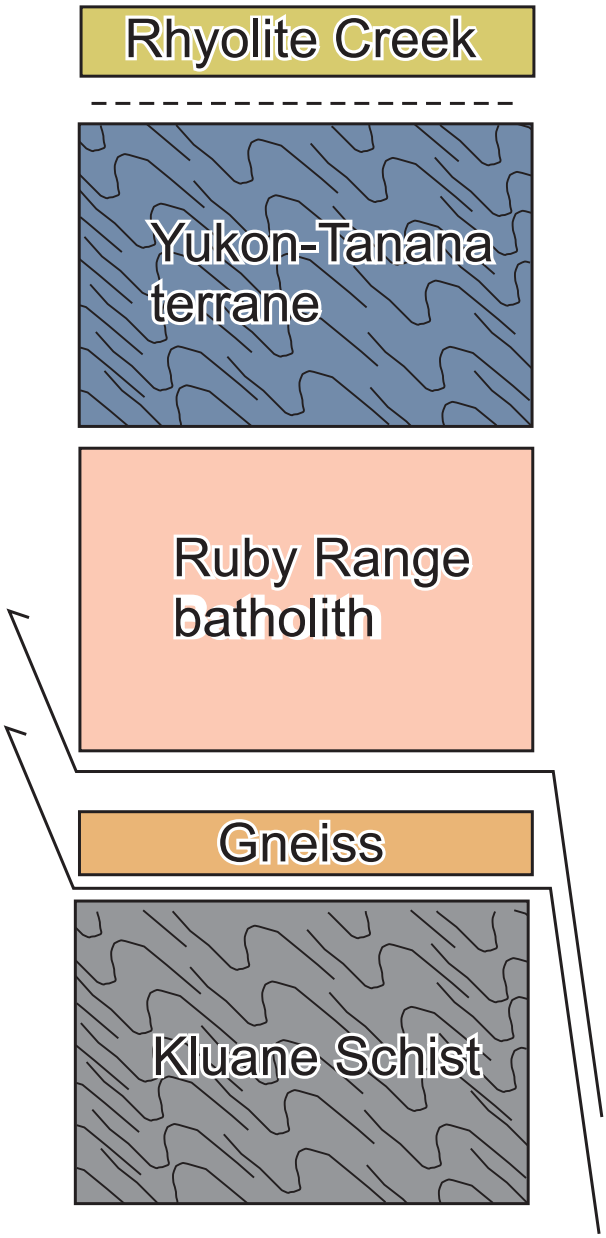

Figure 3. *Schematic stratigraphic column showing general structural relationships. See Figure 2 for lithologic descriptions. Ruby Range batholith is in structural contact with the gneiss and Kluane Schist as well as intrusive into these units.*

Figure 4. *Garnet amphibolite of the Yukon-Tanana terrane, from the northern portion of the project area. Garnet is commonly up to 4 cm in diameter.*

Figure 5. *Grey weathering, variably carbonaceous quartzite of the Yukon-Tanana terrane.*

KLUANE SCHIST

The term Kluane Schist is used to describe the metamorphic rocks found between the Denali fault and the Ruby Range batholith in the southern part of the project area (Fig. 2). They have been referred to as the Kluane metamorphic assemblage (Mezger *et al.*, 2001a) and they make up part of the undivided metamorphic rocks of the Coast plutonic complex of Wheeler and McFeely (1991). The unit is composed primarily of monotonous metapelitic quartz-mica schist; rare bodies of ultramafic rocks and carbonate occur locally. Two separate mappable units were delineated in the present study: a muscovite-rich schist and a biotite-rich schist. Muscovite schist occupies a central position between overlying and underlying (?) domains of biotite schist. Both biotite and muscovite schists are variably carbonaceous, with the amount of carbon decreasing from northwest to southeast. Although generally monotonous, grain size variations occur locally, reflecting primary clastic layering. The transition from biotite to muscovite-rich schist is gradational over several hundred metres and in places difficult to identify due to the alteration and/or the weathering of biotite to a brassy colour.

Muscovite schist is fine to medium-grained and light grey weathering (Figs. 2 and 6). It is generally more carbonaceous than biotite schist, with the amount of carbon increasing to the northwest. Porphyroblasts of plagioclase occur locally and rare garnet is present, generally near late intrusions. Several generations of quartz veins are ubiquitous, locally occurring as quartz-rich layers that parallel the main foliation.

Figure 6. *Grey to beige-weathering muscovite schist typical of the Kluane Schist.*

Biotite schist occurs throughout the southern portion of the map area, surrounding the core of muscovite schist and structurally below the orthogneiss/paragneiss unit. Biotite schist is generally, dark grey to black weathering, fine to medium-grained and consists of biotite ± hornblende and quartz (Fig. 7). Biotite ranges in colour from black to brassy. Locally, garnet is observed both as early, deformed porphyroblasts and as late, overprinting porphyroblasts, the latter generally near crosscutting intrusions. Plagioclase porphyroblasts up to 1 mm are common. Quartz veining is ubiquitous and occurs in several generations.

Carbonate and ultramafic rocks are locally observed interleaved with the schist. Carbonate is light bluish-grey weathering, medium to coarse-grained and laterally discontinuous. Carbonate rocks have been observed in only two localities to date, one just north of Cultus Bay, the other just southwest of Killermun Lake. In both localities they are foliated and metamorphosed and have a distinctive weathering appearance, shown in Figure 8.

Ultramafic rocks occur as discontinuous slivers throughout the Kluane Schist. Individual bodies can reach up to 200 m in structural thickness in the project area. The largest ultramafic body is at Doghead Point (Murphy *et al.*, 2009; Fig. 2), on the northern shore of Kluane Lake between Talbot and Brooks arms. In the study area the ultramafic rocks are mainly serpentinite schist with varying amounts of talc (Fig. 9). Within coarser portions of the schist olivine crystals are preserved. Mezger (2000) interpreted these ultramafic bodies as being part of oceanic crust that was tectonically interleaved with the metasedimentary rocks of the Kluane Schist during accretionary processes.

The age of the Kluane Schist is poorly constrained. The youngest detrital zircons from the Kluane Schist suggest an upper age of deposition of ~95 Ma (see detrital zircon section below). The age the first metamorphic event is around 82 Ma (see detrital zircon section) so deposition must have occurred after 95 Ma and before 82 Ma.

Figure 7. *Dark brown to black-weathering, biotite schist of the Kluane Schist. Here outcrop is cut by late axial-planar cleavage associated with latest phase folding.*

Figure 8. *The rounded edges and smooth erosional troughs are distinctive weathering patterns of carbonate pods found within the Kluane Schist.*

Figure 9. *Strongly deformed and altered ultramafic rock, now essentially a talc schist found within the Kluane Schist.*

GNEISS

Gneiss is found in a continuous belt between the Kluane Schist and lowest portions of the Ruby Range batholith (Fig. 2). The unit can be traced for at least 60 km along strike within the project area. It continues to the southeast and northwest outside of the project area for several 10's of kilometres. The gneiss is fine to medium-grained and banded with melanocratic layers composed of biotite and hornblende, and leucocratic layers consisting of plagioclase, quartz, potassium feldspar and biotite (Fig. 10). It is markedly different in appearance from the

Kluane Schist in that the leucocratic layers are composed of igneous appearing material rather than deformed quartz veins. Garnet is locally abundant and ranges in size from <1 mm to 1 cm. In one exposure, the gneiss is structurally interleaved with very strongly deformed and metamorphosed carbonate horizons (Fig. 11). It is not yet apparent whether the gneiss is a highly metamorphosed equivalent of the Kluane Schist or whether it is a portion of the Yukon-Tanana terrane, or perhaps even the metamorphosed crystalline basement to the Yukon-Tanana terrane. Mezger (2001a) included the gneiss with the Kluane Schist, suggesting they are migmatitic versions of the less metamorphosed schist found away from the Ruby Range contact. Wheeler and McFeely (1991) included the gneiss in the Nisling terrane, now considered part of the Yukon-Tanana terrane. Because of the fault-bound nature of the orthogneiss, it considered a distinct tectonostratigraphic entity in this paper.

RUBY RANGE BATHOLITH

The Ruby Range batholith is a large plutonic complex that is found throughout the central portion of the study area (Fig. 2). Muller (1967) used the term Ruby Range batholith to describe all granitic rocks from the White River southeast to the eastern edge of map sheet 115G. Muller's definition included the main intrusive phase of the batholith between the Kluane Schist and the Yukon-Tanana terrane as well as small, compositionally similar intrusions of unknown age within both the Kluane Schist and the Yukon-Tanana terrane, away from the main core of the complex. We continue this usage but understand that the batholith is a composite body and with more age constraints it may be subdivided into multiple episodes of magmatism.

The Ruby Range batholith is composed largely of quartz-diorite, tonalite and granodiorite with lesser amounts of diorite, gabbro and granite. The base of the Ruby Range batholith is almost entirely characterized by strongly to moderately foliated quartz-diorite that structurally overlies the orthogneiss unit and the Kluane Schist (Fig. 12). The composition becomes more felsic up-section to the north culminating in voluminous amounts of quartz-feldspar porphyry. Several phases of intrusive material can be distinguished purely on crosscutting relationships, and significant evidence for magma mixing can also be observed. Locally, post-tectonic intrusions of unknown age crosscut the foliated phase at the base of the batholith and the underlying orthogneiss unit (Fig. 13). Murphy *et al.* (2009) observed similar relationships outside the study area to the northwest. Several kilometres up from its base, the Ruby Range batholith is relatively undeformed and massive yet still compositionally and texturally variable in that quartz-diorite continues to dominate, but granodiorite and tonalite are common and they are texturally fine-grained to plagioclase and potassium feldspar-porphyritic depending on the composition. Feldspar ranges up to 2 cm in length. The mafic minerals include biotite and hornblende, and magnetite is locally common. Interestingly the presence or absence of magnetite does not appear to be dependant on

Figure 10. *Orthogneiss from the structural top of the Kluane Schist. Leucocratic layers are composed of quartz, plagioclase, biotite and potassium feldspar, while melanocratic layers consist of biotite and hornblende.*

Figure 11. *Strongly deformed and metamorphosed carbonate interleaved with orthogneiss and paragneiss found on the western shore of Talbot Arm.*

composition, but rather is found in all compositions but is not ubiquitous. Tonalite is commonly quartz-porphyritic, with quartz grains up to 0.5 cm and a distinctive smoky grey/blue colour. Miarolitic cavities are common near the upper contact of the batholith where it intrudes Yukon-Tanana terrane. The Ruby Range batholith is only locally foliated near its roof suggesting that much of the accommodated strain within the batholith occurred at its base. Peraluminous quartz-diorite to granodiorite intrusions that include muscovite ± garnet are found within the main batholith, as well as in satellite intrusions well away from the base of the batholith (Fig. 2). These crosscut all ductile structures within the Kluane Schist and are locally mineralized (see below).

Figure 12. *Strongly foliated quartz-diorite typical of the lower contact of the Ruby Range batholith.*

Figure 13. *Massive, undeformed tonalite to granodiorite of the Ruby Range batholith crosscutting fabrics within gneiss of the Kluane Schist.*

Several new U-Pb age determinations suggest a *ca.* 64 to 57 Ma range for the main intrusive phases related to the batholith (Crowley and Murphy, unpublished data; Mortensen and Murphy, unpublished data). The younger ages correspond to the more felsic phases and the older and intermediate ages correspond to more mafic and intermediate phases. Concordant U-Pb ages on zircons from a small boudinaged dyke that cuts the Kluane Schist near the bridge over the Aishihik River, east of Haines Junction, range from 71.8 ± 0.2 to 68.4 ± 0.2 Ma (Fig. 14). This age likely represents a pre-main phase of the Ruby Range batholith.

RHYOLITE CREEK VOLCANO-PLUTONIC COMPLEX

The Rhyolite Creek volcano-plutonic complex refers to the youngest, porphyritic phase of the Ruby Range batholith and its volcanic equivalents. The volcanic rocks were previously included in the Triassic and later (?) unit 4 of Muller (1967) and the Eocene Mount Nansen Group by Tempelman-Kluit (1974). The Mount Nansen Group has since been interpreted as mid-Cretaceous in age (Gordey and Makepeace, 2003) and therefore the volcanic rocks in the project area are no longer considered part of this group. The largest outcrop exposure of this unit in the project area is found in the north, near Rhyolite Creek (Fig. 2). The volcanic rocks consist of intermediate volcanic flows, breccia and tuff, flow-banded rhyolite and felsic tuff, and rare mafic flows, breccia and tuff (Fig. 15). Where volcanic rocks are mafic to intermediate in composition, breccias are almost always found at the base; where felsic, volcanic rocks are usually associated with quartz porphyritic intrusions and dome-like architecture. Porphyritic rocks are purple, brown or beige weathering and contain quartz phenocrysts up to 3 mm in diameter. Quartz porphyritic tonalite occurs extensively, with distinct smokey blue quartz phenocrysts up to 4-5 mm in diameter. The porphyry locally intrudes the overlying volcanic rocks (Fig. 16) and flow-banded rhyolite and quartz-feldspar porphyry from the Rhyolite Creek volcano-plutonic complex are both *ca.* 57 Ma (Crowley and Murphy, unpublished data), affirming the interpretation that porphyries are intruding their coeval volcanic rocks.

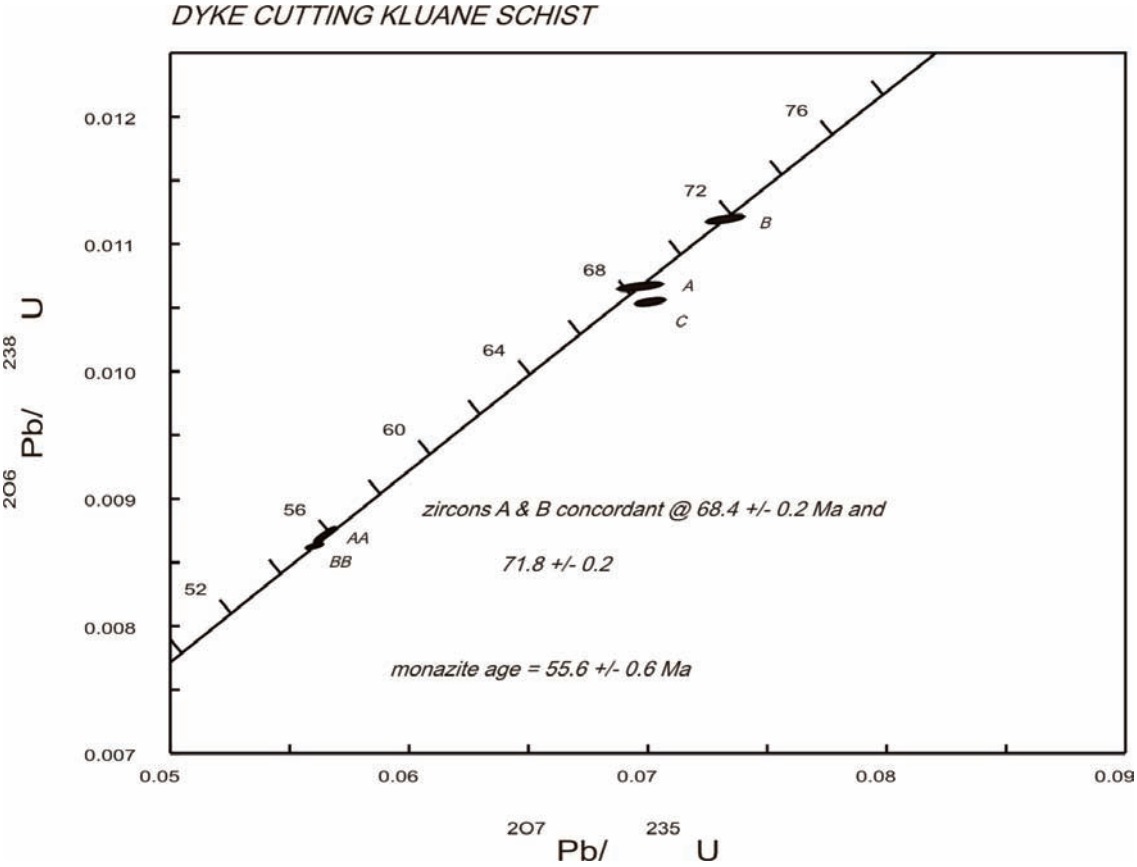

Figure 14. *U-Pb concordia diagram for zircon analyses from a dyke crosscutting main foliation within Kluane Schist. This age likely represents a pre-main Ruby Range batholith phase.*

Figure 15*. Flow banded rhyolite of the Rhyolite Creek volcano-plutonic complex.*

Figure 16. *Flow banded rhyolite being intruded by quartz, feldspar porphyry. The deformation of the flow bands suggest that the rhyolite was not completely cooled before intrusion.*

DETRITAL ZIRCON ANALYSES

Detrital zircon U-Pb analyses were performed on samples from the Kluane Schist to investigate provenance variations and constrain the age of deposition. Two samples were analysed, one without the benefit of cathodoluminescent and backscatter imaging, at the Pacific Centre for Isotopic and Geochemical Research (PCIGR; 08DM126) at the University of British Columbia and one, with imaging, at the Inco Innovation Centre (IIC), Memorial University, St Johns', Newfoundland (09SIT11). Through detailed imaging and subsequent core and rim analyses of sample 09SIT11, we were able to ascertain information relating to provenance and the maximum age for the onset of sedimentation. In addition, we constrained the ages of subsequent thermal events that resulted in extensive Pb loss of the primary detrital zircon population. The following discussion relies predominantly on data collected from sample 09SIT11; however, we provide a comparison of the two samples to highlight the similar provenance variations and the overlap between the ages of youngest accurate detrital zircon populations, after removal of metamorphic ages from the detrital dataset.

ANALYTICAL METHODS

Sample preparation and U-Pb Laser Ablation Microprobe Inductively Coupled Plasma Mass Spectrometry (LAM ICP-MS) geochronology for sample 09SIT11 was completed at the IIC, St Johns', Newfoundland. A detailed outline of the methodology is given in Bennett and Tubrett (2010). U-Pb data are reported in Appendix 1. Zircon separates were extracted using standard crushing techniques, and heavy mineral concentrates were produced using a Wilfley™ table and heavy liquids. To minimize sampling bias, we created a single zircon fraction by doing the initial stages of magnetic separation (Frantz™ isodynamic separator) only, to remove unwanted silicate and accessory phases (*e.g.*, monazite, titanite, garnet). Sampling bias was also minimized by randomly dumping zircon separates onto a grain-mount, as opposed to hand-picking particular grains of interest. Detrital zircon grains were photographed in transmitted light and subsequently mounted in epoxy resin and polished to expose grain cores. Grain mounts were then carbon coated and imaged using backscattered electron (BSE) and cathodoluminescence (CL) image analysis (Fig. 17). Approximately 200 zircon grains were mounted and imaged. Image analysis of 09SIT11 demonstrates variable growth of metamorphic zircon on

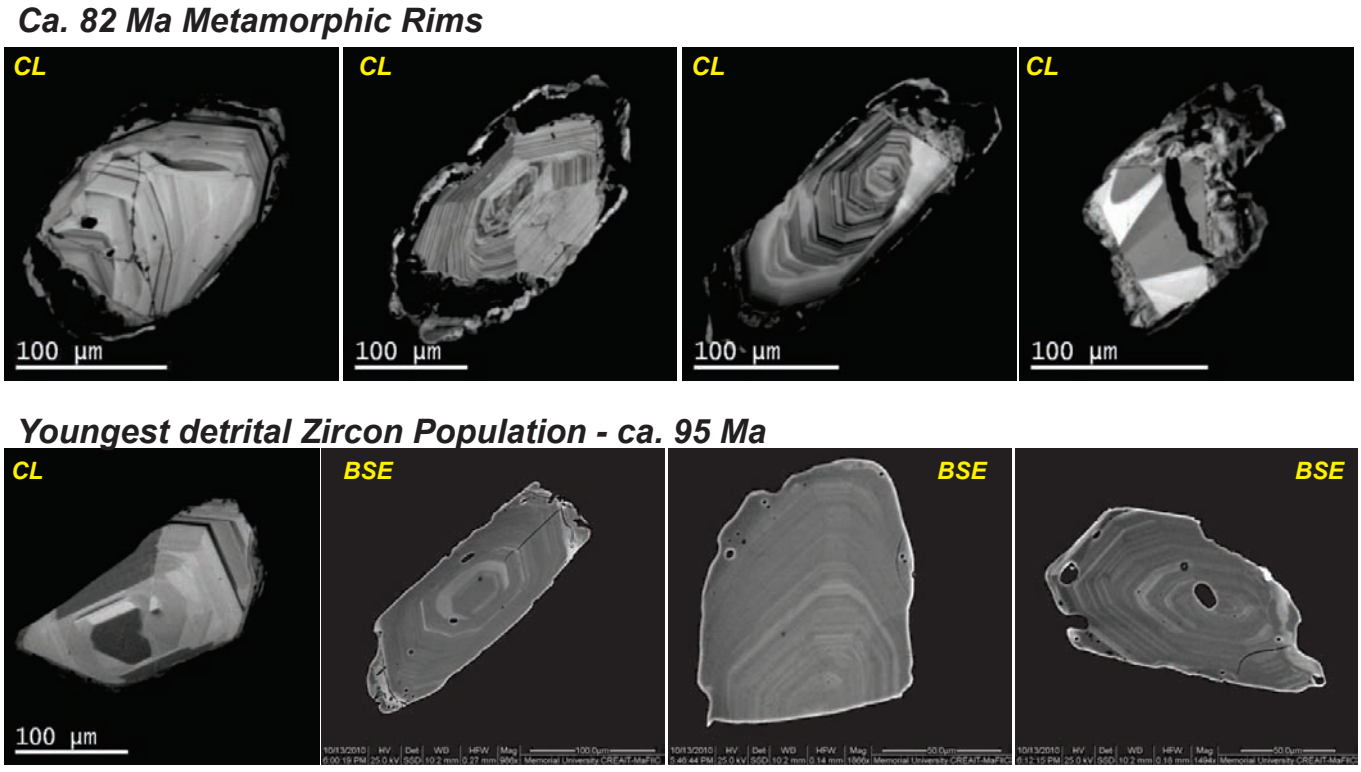

Figure 17. *Cathodoluminescence (CL) and backscatter electron (BSE) images of detrital zircons from sample 09SIT11. Metamorphic rims are the black areas between bright cores and rims. Note the lack of metamorphic rims on the youngest detrital zircons at bottom.*

detrital zircon grains (Fig. 17). A clear understanding of these zircon epitaxial relationships (core *vs.* rim) occurring within 09SIT11 assisted intragrain placement of the laser beam during data collection, which ensured analysis of single discrete age domains (*i.e.*, detrital *vs.* metamorphic) rather than overlapping or mixed age domains. Analysis of multiple age domains within a single zircon grain produces isotopically heterogeneous data which, typically, is a significant contributor to U-Pb discordance using the LAM ICP-MS technique.

Completing U-Pb analyses using LAM ICP-MS for 09SIT11 proved challenging due to the low Pb and U concentrations in grains which had undergone partial to complete Pb loss as a result of younger metamorphic events. In order to acquire useable age data for these grains, background U and Pb levels within the instrument were required to be at their lowest. Additionally, higher laser energy was applied (up to 5J) to analyse the low Pb and U grains to achieve useable, but lower precision age data. For analyses where ^{207}Pb intensity did not exceed background levels, inaccurate and meaningless $^{207}Pb/^{235}U$ ages result. Consequently, an assessment of concordance could not be made. These data were not included in the final detrital zircon population as the accuracy of the $^{206}Pb/^{238}U$ could not be determined (*i.e.*, Pb loss or detrital age). The dataset has also been filtered to exclude data exhibiting greater than 10% discordance. Additionally, during data collection the isotope mass 204 (Hg204+Pb204) was monitored. For any individual analysis, where 204 levels exceeded acceptable background levels the data were rejected from the final dataset as these grains have excess common Pb.

The interpreted maximum age of the onset of sedimentation of the sampled bed and the overprinting metamorphic ages for 09SIT11 are based on calculations of concordia ages from individual U-Pb isotopic analyses that have a probability of concordance greater than 0.20 (see Bennett and Tubrett, 2010; Fig. 18). Two-sigma uncertainty levels are reported for all calculated ages and plotted on concordia, unless stated otherwise. Final age calculations include U decay constant uncertainties, which are plotted graphically on concordia plots. Concordia were calculated using Ludwig (1999). Uranium and thorium concentration data and Th/U ratios are also calculated for each zircon analysed in 09SIT11 and reported in Appendix 1. One hundred and thirty-two analyses were completed on 125 zircon grains, 116 from detrital cores and 16 from younger metamorphic rims. Twenty core analyses exceeded the 10% discordance filter

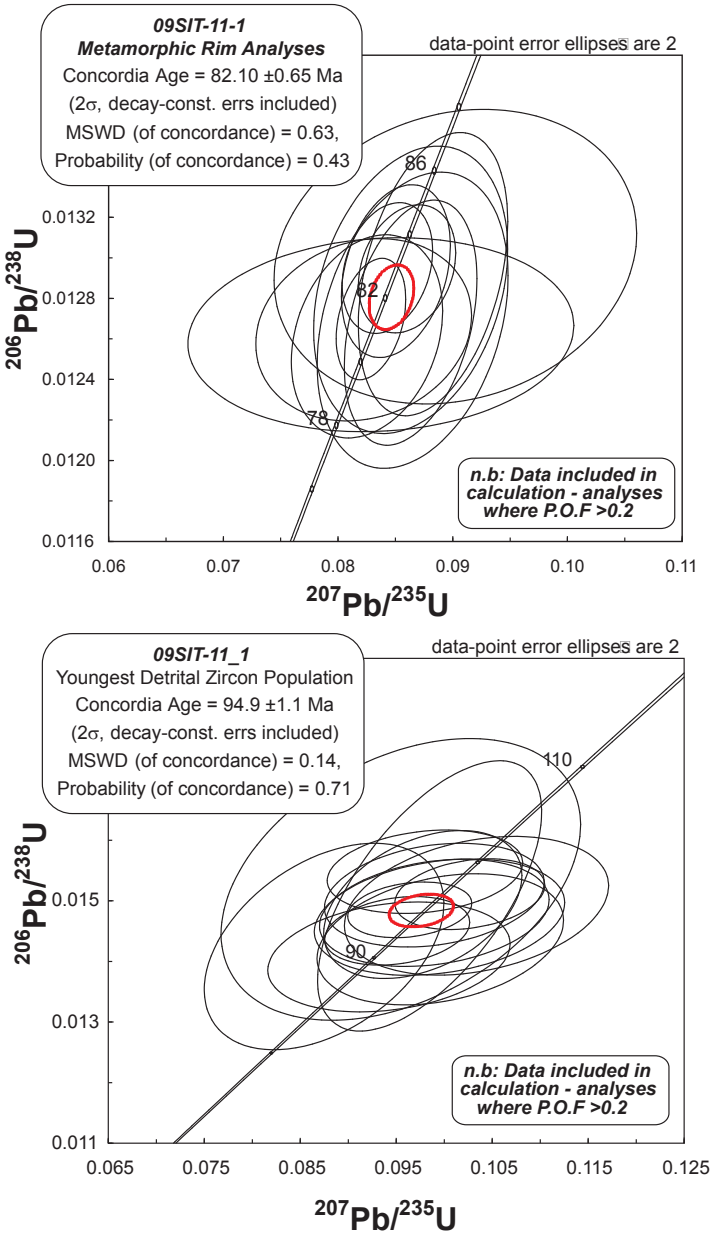

Figure 18. *U-Pb concordia plots from detrital sample 09SIT11;* ***(a)*** *analyses of metamorphic rims, and* ***(b)*** *analyses of the youngest detrital zircons.*

and were excluded from the dataset. Strong Pb loss had affected 22 zircon cores and analyses produced inaccurate and/or meaningless $^{207}Pb/^{235}U$ ages; these results were subsequently excluded from the final dataset. U-Pb data for the remaining 71 core analyses are presented in Figure 19. U-Pb age data collected for high mean atomic number metamorphic rims and grains interpreted from BSE images to represent new metamorphic zircon growth are presented in Figure 18a.

PROVENANCE OF THE KLUANE SCHIST

Complete detrital populations for both 09SIT11 and 08DM126 are illustrated in Figure 19. The data highlight the predominance of Phanerozoic grains, with subordinate populations occurring at *ca.* 1.2 Ga, 1.8 Ga and a single Archean grain from 09SIT11 (Appendices 1 and 2). Closer examination of the Phanerozoic populations reveals discrete age peaks at ~100 Ma, 200 Ma and 325-350 Ma, with subordinate ages from both samples occurring between the 100 and 220 Ma peaks (Fig. 20).

The detrital age populations in the Kluane Schist from both samples compare closely with known igneous ages from nearby terranes, suggesting that they formed the source area from which these zircons were eroded. The Proterozoic and Archean ages are significant detrital peaks within the Yukon-Tanana terrane (Colpron *et al.*, 2006). The 350-325 Ma ages from the detrital population are also a well-represented igneous age in Yukon-Tanana terrane (Nelson *et al.*, 2006; Piercey *et al.*, 2006). The ages spanning from ~220 to ~100 Ma are all well-represented within the Aishihik batholith (*ca.* 190-180 Ma) and the Coast plutonic complex (Late Triassic to Eocene; Johnston and Erdmer, 1995a; Gehrels *et al.*, 2009). LAM ICP-MS U-Pb ages ranging from 98 Ma and 104 Ma have been obtained from the Nisling Range granodiorite located about 60 km north-northwest of the study area (Mortensen and Murphy, unpublished data; Tubrett and Murphy, unpublished data). Interestingly, Mezger (2001b), suggested that the only group of rocks in the vicinity that has the same geochemical and isotopic signature of the Kluane Schist is the Nisling Range granodiorite.

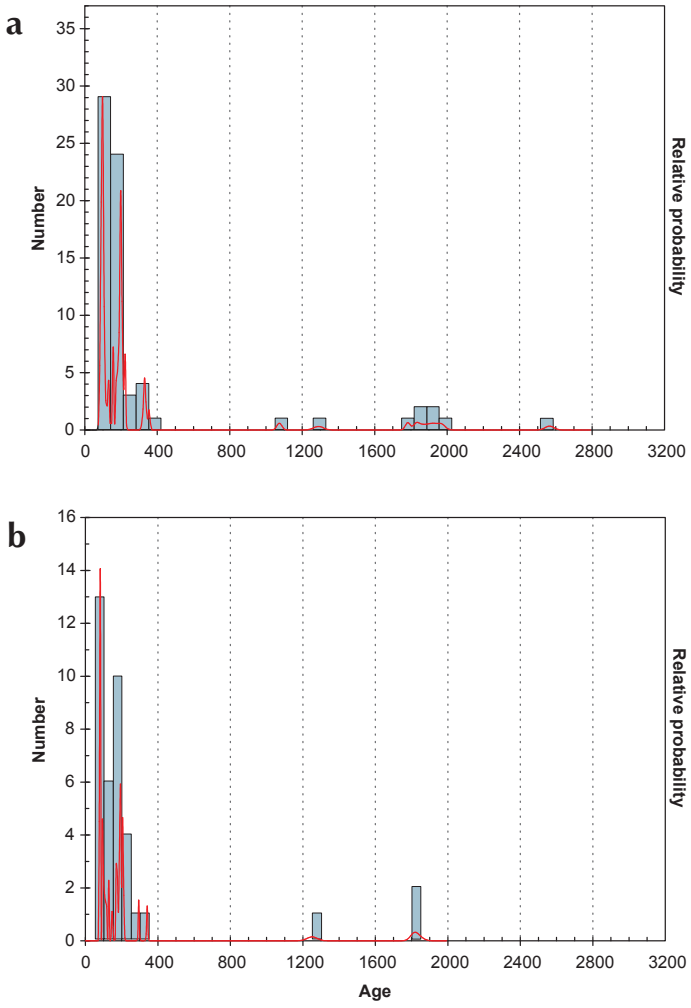

Figure 19. *Probability density plots of two detrital zircon samples from the Kluane Schist;* ***(a)*** *sample 09SIT11, and* ***(b)*** *sample 08DM126.*

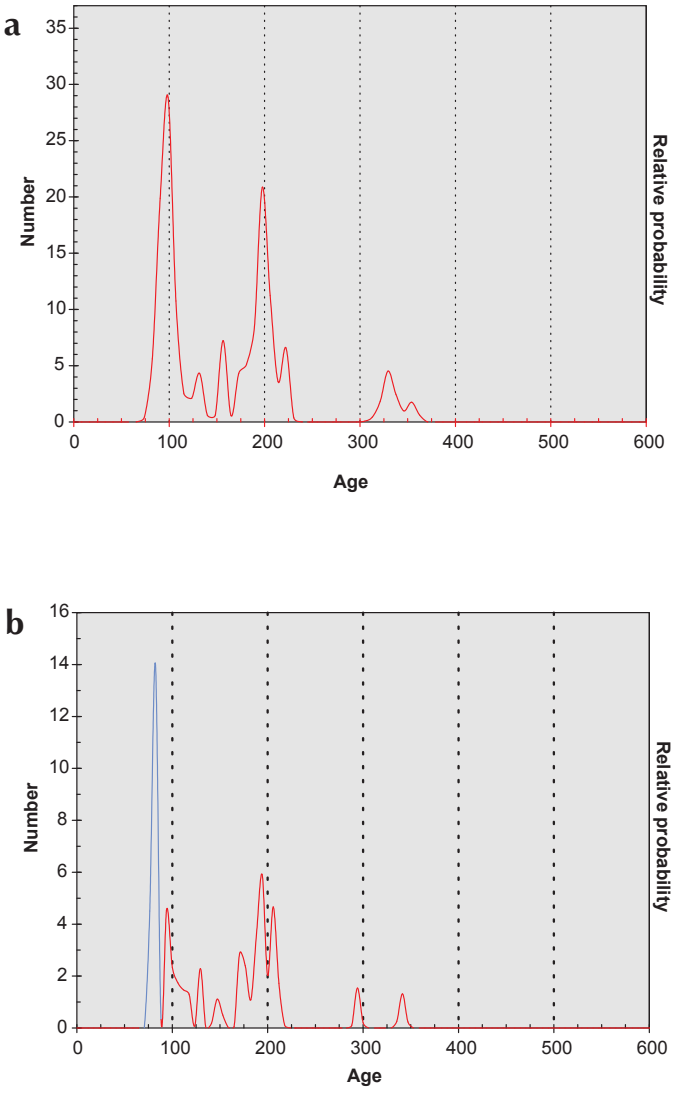

Figure 20. *Probability density plots of ages of detrital zircons from the Kluane Schist, showing only the Phanerozoic ages.* ***(a)*** *sample 09SIT11, and* ***(b)*** *sample 08DM126, the blue peak represents the metamorphic ages from the sample.*

AGE OF DEPOSITION AND METAMORPHISM OF THE KLUANE SCHIST

Variable development of metamorphic overgrowth rims is apparent from the images shown in Figure 17. These metamorphic growth zones correspond to domains characterized by high concentrations of U (879–8129 ppm) and very low Th (4-88 ppm; Appendix 1). Analysis of the high U/low Th metamorphic rims yielded a concordia age of 82.10 ± 0.65 Ma (Fig. 18A). Metamorphic ages determined from zircon rims in sample 09SIT11 correlate with the youngest age peak determined for sample 08DM126. Consequently we interpret the youngest age peak in 08DM126 as a metamorphic age rather a detrital age (Fig. 20).

The distinctive high U and low Th composition of the metamorphic growth zones was an important criterion in discriminating them from primary detrital grains. Grains that are detrital in origin were typically characterized by higher concentrations of Th and lower U values. Correspondingly, zircon grains without significant growth of younger metamorphic zircon preserved the original internal zoning structures (*e.g.*, oscillatory, sector, diffuse; Fig. 17). The youngest accurate age from this population of detrital grains from sample 09SIT11 is 94.9 ± 1.1 Ma (Fig. 18b). After stripping away the metamorphic peak from 08DM126 the age of the youngest peak is very close to the ~95 Ma age for the youngest detrital grain from 09SIT11 (Fig. 20b). We therefore interpret this age as the maximum age of the onset of deposition of this part of the Kluane Schist.

STRUCTURAL GEOMETRY AND RELATIONSHIPS

The project area is characterized by three separate fault-bound domains that include, from highest structural level to lowest, the Yukon-Tanana terrane, the gneiss unit, and the Kluane Schist (Fig. 21). We consider the Ruby Range batholith to be a late kinematic intrusion that overprints the original structural contact between the Yukon-Tanana terrane, the orthogneiss and the Kluane Schist. The structural character of each domain is described separately below. The relationships between each domain are discussed in the context of younger structural elements that affect all domains.

YUKON-TANANA TERRANE

Structural trends within the Yukon-Tanana terrane generally define a northeast-dipping structural panel of Paleozoic rocks that is interpreted to be in thrust contact with underlying gneiss and/or the Late Cretaceous Kluane Schist. The lower contact of the Yukon-Tanana terrane is obscured by the Ruby Range batholith. Pre-Jurassic and Jurassic deformation and metamorphism within the Yukon-Tanana terrane was responsible for the initial northeast to east dip of the main foliations (Johnston and Erdmer, 1995a). These foliations have been kinked and overprinted by lower grade metamorphism related to thrusting over the Kluane Schist and intrusion of the Ruby Range batholith (Johnston and Erdmer, 1995a). More than one phase of folding is evident. The first phase is related to pre-Jurassic deformation, with later isoclinal re-folding of these during the Jurassic (Johnston and Erdmer, 1995a; Johnston and Erdmer, 1995b). The resulting folds generally verge to the southwest, with plunges towards both the northwest and southeast with some folds verging to the northeast. Stretching lineations occur on northeast dipping foliations; these trend towards the northeast; however, these are likely related to Jurassic deformation and syn-tectonic intrusion of the Aishihik batholith (Johnston and Erdmer, 1995a).

KLUANE SCHIST

Deformation within the Kluane Schist is expressed by a pervasive northwest-striking, northeast-dipping foliation. This foliation is likely a composite of two progressive phases of deformation related to southwest-verging deformation associated with thrusting of Yukon-Tanana terrane over the Kluane Schist. It is difficult to see

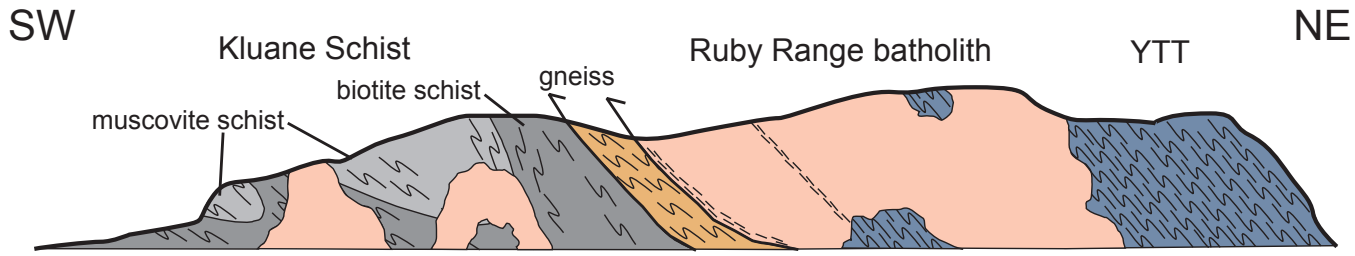

Figure 21. *Schematic cross section drawn from southwest to northeast, through the middle of the Coast Belt project area.*

these folds in outcrop and they are best observed in F2 fold hinges or expressed by pre and syn-deformation quartz veins (Fig. 22). These quartz veins are commonly boudinaged and tight to isoclinally folded and refolded. In the southeastern exposure of the Kluane Schist, late-stage south-to-southeast trending open-to-closed folds of the main foliation are preserved (Fig. 23). These late folds deform the main foliation so that it locally dips towards the southeast and southwest rather than the northeast. Timing of these structures is not well constrained. They must be post-95 Ma, the maximum depositional age of the Kluane Schist, and pre-57 Ma, the age for crosscutting porphyritic dykes. The 84 Ma metamorphic overgrowths on the detrital zircons likely reflect the main metamorphic event related to thrusting of Yukon-Tanana over the Kluane Schist. The early northeast-dipping foliation is most certainly related to this event and, as this foliation is seemingly crosscut by a 70 Ma late-syn-kinematic dyke (at the Aishihik River), southwestward thrusting was likely over by this time.

ORTHOGNEISS/PARAGNEISS

The structural relationships within the orthogneiss unit and its relationships with the other domains are not clear. The contact with the underlying Kluane Schist is interpreted as a north to northeast-dipping shear zone, based upon an increase in intensity of fabrics towards to the lower contact of the gneisses. The upper contact is either a shear zone that places strongly deformed Ruby Range quartz diorite over the gneiss or an intrusive contact where younger phases of the batholith crosscut both sheared quartz diorite and orthogneiss. Rootless, isoclinal, southwest-verging folds within the orthogneiss/paragneiss unit are ubiquitous and help define the overall northeast dip of the penetrative foliation. Locally the main foliation is quite discordant with the sheared base, suggesting a more complex nature to the internal structural relationship.

RUBY RANGE BATHOLITH

Structural relationships within the Ruby Range batholith are purely time dependant, in that earlier phases are foliated and are therefore interpreted as pre to syn-tectonic, whereas later phases crosscut earlier formed fabrics and are interpreted as post-tectonic. Fabrics within the Ruby Range batholith are most strongly developed at the base of the batholith where it is in contact with the gneiss unit. The textures of the fabrics grade from proto-mylonitic and gneissic to magmatic away from the base. A magmatic age from an early, foliated phase of the Ruby Range batholith suggests that deformation was occurring at *ca.* 64 Ma (Crowley and Murphy, unpublished data). As mentioned earlier, it is likely that deformation between the Yukon-Tanana terrane and the Kluane Schist was taking place prior to intrusion of the main phase of the Ruby Range batholith, based on the Late Cretaceous age from a boudinaged dyke from the Aishihik River and *ca.* 84 and 70 Ma metamorphic overprints on detrital grains from the Kluane Schist.

Figure 22. *Tight to isoclinally folded quartz veins found within the Kluane Schist. These folds are likely F2 regional folds.*

Figure 23. *Late F3 folds within the Kluane Schist. These folds verge to the west-southwest.*

POST-64 MA DEFORMATION

Faults in the area are not well exposed, as they generally occur in the heavily overburdened filled valleys. The steep, regionally crosscutting faults are imaged on the regional and finer scale aeromagnetic surveys over the project area, and some are defined based on discontinuities in rock types and structures across valleys. The largest of these structures is the Denali fault, found in the southwestern-most portion of the field area. This structure has accommodated at least 450 km of right-lateral offset, likely in the latest Cretaceous to Eocene (Eisbacher, 1976; Lowey, 1998). North to northeast and northwest-striking faults are common, many of which do not penetrate the base of the Ruby Range batholith (Fig. 2). Kinematic interpretation of these structures is difficult to resolve because of a lack of good marker horizons. Similar fault patterns are observed to the northwest of the study area and have been interpreted to be related to hangingwall damage during pluton emplacement over the Kluane Schist (Murphy, 2007; Murphy *et al.*, 2008). These faults are likely important for mineralization as many of the gold bearing quartz-carbonate veins near Killermun Lake are found within north to northeast-striking structural zones (Wengzynowski, 1995; Eaton, 2003). East-striking faults cut by the Denali fault dissect the southern part of the project area and are interpreted to crosscut young, unfoliated phases of the Ruby Range batholith and some of the north-striking faults (Fig. 2).

Preliminary results from bedrock mapping and geochronological studies within the Coast Belt area of southwest Yukon indicate that the present day structural stacking and lithotectonic relationships are the result of southwestward (today's coordinates) thrusting of Yukon-Tanana terrane over the Kluane Schist and syn to post-tectonic intrusion of the main phase of the Ruby Range batholith. The *ca.* 70 Ma age from the boudinaged dyke near Aishihik River that crosscuts the main foliation in the Kluane Schist suggests that deformation related to thrusting was well underway by this time. The age of the dyke coincides with some metamorphic rims and some completely reset detrital grains from the Kluane Schist. Given that deposition of the Kluane Schist likely is constrained to post-*ca.* 95 Ma there is a maximum window of 25 My between deposition and peak (?) metamorphism of the Kluane Schist. Intrusion of the earliest dated phase of the Ruby Range batholith occurred late in the deformational history, at least 6 My after the boudinaging of the dyke at *ca.* 64 Ma (Crowley and Murphy, unpublished data). It is possible that much of the later strain was accommodated near the base of the intruding batholith in the Paleocene. Later stage intrusions that crosscut foliation in the Kluane Schist appear to be more peraluminous in composition and may reflect the tapping of a different source of magma along deep penetrating faults like the Denali fault and related structures.

METALLOGENIC IMPLICATIONS

Mineral potential in the project area is separated into two generalized categories: 1) porphyry and epithermal mineralization; and 2) orogenic gold.

PORPHYRY/EPITHERMAL OCCURRENCES

In the early 1970's a few companies had small exploration programs within the project area focussing mainly on Casino type Cu-Mo porphyries. These programs included only limited drilling and geochemical and geological ground surveys and assaying was restricted to molybdenum and copper (*e.g.*, Smith, 1971; Trigg, Woolet and Associates, 1971). From this era several new Cu-Mo porphyry showings were identified in the upper portion of the Ruby Range batholith and overlying Yukon-Tanana terrane. The newly-recognized crustal section described here allows for a more comprehensive look at the porphyry and epithermal potential of the area, as the geologic setting and structural levels of the batholith are better understood.

Widespread, mainly potassic and localized silicic alteration associated with the Raft Creek/Meloy prospect (Yukon MINFILE 115G070) near the top of the Ruby Range batholith is highly visible from the surrounding ridges and mountain tops. Similar reddish colour anomalies can be seen in other areas along the top of the Ruby Range batholith. Most of these are associated with other MINFILE occurrences. At the time of discovery, these mineral occurrences were described as Cu-Mo-Au porphyry systems similar to the Casino deposit located northwest of the study area. The occurrences in the study area are associated with the upper-most fractionated portion of the Ruby Range batholith, which is now known to be younger than Casino mineralization. At least one of the younger (based on crosscutting relationships with the Kluane Schist), peraluminous intrusions is known to host significant mineralization. An example of this late mineralization was discovered in a quarry along the Alaska Highway late in the field season. The occurrence consists of molybdenite, which occurs along a series of altered subvertical joint surfaces in the southern part of the project area (Fig. 24).

Silica ± potassic alteration was observed at the plutonic-volcanic transition (Fig. 25) in the upper part of the batholith. This alteration has the appearance of high sulfidation, epithermal style mineralization, found above and adjacent to deeper porphyry systems. The silica alteration is likely the result of highly acidic, low pH fluids infiltrating the host rock, dissolving everything but the silica.

Figure 24. *Parallel, strongly altered joint surfaces found in a peraluminous intrusion found within a quarry along the Alaska Highway. Molybdenum mineralization is often found within the alteration zones.*

Figure 25. *Massive silica alteration of quartz-feldspar porphyry from the top of the Ruby Range batholith. The alteration is likely the result of a high sulfidation epithermal system.*

OROGENIC GOLD - ANALOGIES WITH JUNEAU GOLD BELT

The tectonic framework observed within the project area is very similar to that of the Juneau Gold Belt in southeast Alaska (Fig. 26). In Alaska, around Juneau, the east-west juxtaposition of terranes includes the Yukon-Tanana terrane, thrust to the west over the late Paleozoic Taku terrane (a Late Paleozoic to Triassic metasedimentary and metavolcanic assemblage), which is itself thrust over the Jura-Cretaceous sedimentary rocks of the Gravina belt (McClelland and Mattinson, 2000; Miller *et al.*, 2000). Paleocene to Eocene intrusive rocks of the Coast plutonic complex occur between the Yukon-Tanana rocks and the Taku terrane. These plutonic rocks are thought to have intruded during deformation. Gold mineralization has been found in abundance within the plutonic rocks, leading to the use of the term Juneau gold belt when describing the metallogenic character of the area (Goldfarb *et al.*, 1988).

Southwestern Yukon comprises lithotectonic panels of similar age and affinity to those in southeastern Alaska, and preserves the same structural juxtaposition, with Yukon-Tanana terrane being thrust to the southwest over rocks of the Kluane Schist (Taku terrane analog). The Kluane Schist is interpreted to have been thrust to the southwest over Jura-Cretaceous rocks of the Dezadeash Formation. The Ruby Range batholith is age-equivalent to the Coast plutonic complex, and occurs at the same structural level as the complex.

The similarities between the two areas are striking and a metallogenic comparison between the two areas has previously been suggested (Wengzynowski, 1995). In southeastern Alaska there has been mining of several gold deposits for about 100 years, the most recent, the Kensington mine, opening in 2010. The numerous deposits have been interpreted as orogenic gold systems directly related to the tectonic processes active in southeast Alaska during the latest Cretaceous to Eocene (Miller *et al.*, 1994; Miller *et al.*, 1995). A generalized description of orogenic gold systems is one where regional hydrothermal fluids focus within crustal weaknesses in metamorphic rocks that are spatially associated with large-scale compressional to transpressional structures and abundant syn-tectonic plutonism (Groves *et al.*, 1998; Goldfarb *et al.*, 2001). The deposits typically consist of abundant quartz-carbonate veins formed over a broad range of temperatures and pressures, somewhere between 200-650°C and 1-5 kbar (Groves, 1993). The veins generally form late in the deformational-metamorphic-magmatic evolution and

mineralization is strongly structurally controlled, related to faults, shear zones and folds (Hodges, 1989; Groves *et al.*, 2003).

Known lode-gold occurrences in the Kluane Schist, although not well studied, have characteristics indicative of orogenic style mineralization. The vein system at Rockhaven Resources Ltd. Kluane project (Yukon MINFILE 115H 055, 115H 047) shares many of the characteristics of the orogenic-type gold veins found in the Juneau gold belt. Quartz-carbonate ± muscovite, arsenopyrite veins that host gold mineralization in the Kluane Schist have been described by Wengzynowski (1995) and Eaton (2003), and are similar to those observed within the Juneau gold belt (Miller *et al.*, 1995).

CONCLUSIONS

While only one summer of mapping has been completed in the area and most analytical data are not yet available to evaluate, a number of conclusions can be drawn from the work completed to date:

1. The structural stacking of the tectonic elements creates an exposed section of crust roughly 40 km thick. This section includes an entire batholith from its roots up into the porphyry and epithermal realms, and its overlying volcanic carapace.
2. The Ruby Range batholith is syn-to-post tectonic and becomes more felsic higher in the crustal section.
3. A unit of orthogneiss/paragneiss of uncertain age and correlation occurs along the base of the batholith and structurally above the Kluane Schist.

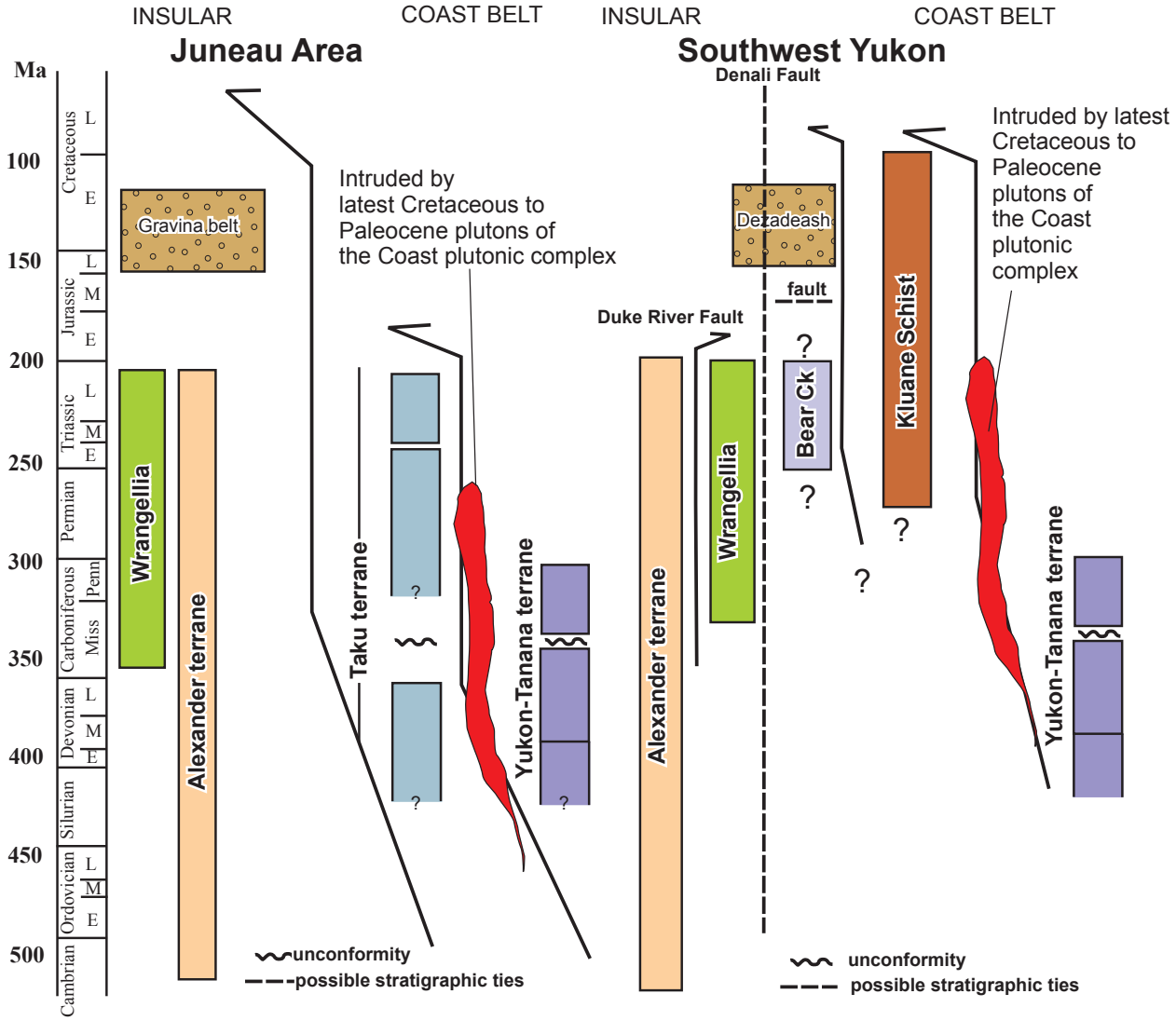

Figure 26. *Schematic stratigraphic sections from the Juneau area, southeast Alaska and the Coast Belt area,southwest Yukon. Alaska data modified from McClelland and Mattinson (2000) and Miller et al. (2000).*

4. The potential for porphyry and epithermal style mineralization increases up crustal section.
5. The depositional age of the Kluane Schist is constrained by detrital zircons as young as ~95 Ma. The provenance of the Kluane Schist is likely an uplifted Yukon-Tanana terrane and Jurassic to Cretaceous plutons of the Aishihik batholith and the Coast plutonic complex.
6. LA-ICPMS dating of metamorphic rims on Kluane Schist detrital zircons suggest that metamorphism significantly intense enough to cause Pb loss and new zircon growth occurred at ~82 Ma and ~70 Ma.
7. The lithotectonic relationships observed in southwestern Yukon are similar to those in southeastern Alaska, increasing the potential for orogenic-style gold mineralization.

ACKNOWLEDGEMENTS

The authors would like to thank Maurice Colpron for a thorough review of this paper. S.I. would like to thank the Coast Belt crew, Megan Routley, Rosie Cobbett, Liz Westberg, Ben Stanley, Sarah Shoniker, Amber Blackwell, Abe Torchinsky and Ryan Pippy, for never complaining and working so hard. We thank Helidynamics and Trans North Helicopters for excellent, reliable and safe service. Thanks to Lance Goodwin and Sian Williams for an excellent camp and great atmosphere.

REFERENCES

Bennett, V. and Tubrett, M., 2010. U-Pb isotopic age dating by LAM ICP-MS, INCO Innovation Centre, Memorial University: Sample preparation methodology and analytical techniques. *In:* Yukon Exploration and Geology 2009, K.E. MacFarlane, L.H. Weston and L.R. Blackburn (eds.), Yukon Geological Survey, p. 47-55.

Colpron, M., Mortensen, J.K., Gehrels, G.E. and Villeneuve, M.E., 2006. Basement complex, Carboniferous magmatic arcs and Paleozoic deformation in Yukon-Tanana terrane of central Yukon: Field, geochemical and geochronological constraints from Glenlyon map area. *In:* Paleozoic evolution and metallogeny of pericratonic terranes at the ancient Pacific margin of North America, Canadian and Alaskan Cordillera, M. Colpron and J.L. Nelson (eds.), Geological Association of Canada, Special Paper 45, p. 131-152.

Eaton, W.D., 2003. Hand trenching, propecting and soil geochemistry at the Ruby Range Project. Yukon Territorial Assessment Report 094415, 102 p.

Eisbacher, G.H., 1976. Sedimentology of the Dezadeash flysch and its implications for strike-slip faulting along the Denali fault, Yukon Territory and Alaska. Canadian Journal of Earth Sciences, vol. 13, p. 1495-1513.

Erdmer, P., 1991. Metamorphic terrane east of Denali fault between Kluane Lake and Kusawa Lake, Yukon Territory. *In:* Current Research, Part A, Geological Survey of Canada, Paper 91-1A, p. 37-42.

Erdmer, P. and Mortensen, J.K., 1993. A 1200-km-long Eocene metamorphic-plutonic belt in the northwestern Cordillera: Evidence from southwet Yukon. Geology, vol. 21, p. 1039-1042.

Gehrels, G.E., Rusmore, M.E., Woodsworth, G.J., Crawford, M.L., Andronicos, C.L., Hollister, L.S., Patchett, P.J., Ducea, M., Butler, R.F., Klepeis, K.A., Davidson, C., Friedman, R.M., Haggart, J., Mahoney, J.B., Crawford, W.A., Pearson, D. and Girardi, J., 2009. U-Th-Pb geochronology of the Coast Mountains batholith in north-coastal British Columbia: Constraints on age and tectonic evolution. Geological Society of America Bulletin, vol. 121, p. 1341-1361.

Goldfarb, R.J., Groves, D.I. and Gardoll, S., 2001. Orogenic gold and geologic time: a global perspective. Ore Geology Reviews, vol. 18, p. 1-75.

Goldfarb, R.J., Leach, D.L., Pickthorn, W.J. and Paterson, C.J., 1988. Orogin of lode-gold deposits in the Juneau gold belt, southeastern Alaska. Geology, vol. 16, p. 440-443.

Gordey, S.P. and Makepeace, A.J., 2003. Yukon Digital Geology (version 2). Geological Survey of Canada, Open File 1749.

Groves, D.I., 1993. The crustal continuum model for the late-Archean lode-gold deposits of the Yilgarn Block, Western Australia. Mineralia Deposita, vol. 28, p. 366-374.

Groves, D.I., Goldfarb, R.J., Robert, F. and Hart, C.J.R., 2003. Gold deposits in metamorphic belts: Overview of current understanding, outstanding problems, future research, and exploration significance. Economic Geology, vol. 98, p. 1-29.

Groves, D.I., Goldfarb, R.J., Grebre-Mariam, H., Hagemann, S.G. and Robert, F., 1998. Orogenic gold deposits-a proposed classification in the context of their crustal distribution and relationship to other gold deposit type. Ore Geology Reviews, vol. 13, p. 7-27.

Hodges, C.J., 1989. The structure of shear-related, vein-type gold deposits: A review. Ore Geology Reviews, vol. 4, p. 231-273.

Johnston, S.T. and Timmerman, J.R., 1994. Geology of the Aishihik Lake and Hopkins Lake map areas (115H6/7), southwestern Yukon. *In:* Yukon Exploration and Geology 1993, S.R. Morison (ed.), Indian and Northern affairs Canada, Exploration and Geological Services Division, p. 93-110.

Johnston, S.T. and Erdmer, P., 1995a. Hot-side-up aureole in southwest Yukon and limits on terrane assembly of the northern Canadian Cordillera. Geology, vol. 23, p. 419-422.

Johnston, S.T. and Erdmer, P., 1995b. Magmatic flow and emplacement foliations in the Early Jurassic Aishihik batholith, southwest Yukon: Implications for northern Stikinia. *In:* Jurassic magmatism and tectonics of the North American Cordillera, D.M. Miller and C. Busby (eds.), Geological Society of America, Special Paper 299, p. 65-82.

Johnston, S.T. and Canil, D., 2006. Crustal architecture of SW Yukon, northern Cordillera: Implications for crustal growth in a convergent margin orogen. Tectonics, vol. 26, p. 18.

Johnston, S.T., Mortensen, J.K. and Erdmer, P., 1996. Igneous and meta-igneous age constraints for the Aishihik metamorphic suite, southwest Yukon. Canadian Journal of Earth Sciences, vol. 33, p. 1543-1555.

Kiss, F., 2010. Residual total magnetic field, Kluane area aeromagnetic survey, Parts of NTS 115A, 115B, 115G and 115H, Yukon. Geological Survey of Canada, Open Files 6584 to 6591; Yukon Geological Survey Open Files 2010-21 to 2010-28.

Lowey, G., 1998. A new estimate of the amount of displacement on the Denali Fault system based on the occurence of carbonate megaboulders in the Dezadeash Formation (Jura-Cretaceous), Yukon, and the Nutzotin Mountains sequence (Jura-Cretaceous), Alaska. Bulletin of Canadian Petroleum Geology, vol. 46, p. 379-386.

Ludwig, K.R., 1999. IsoplotEX v.2.6. Berkeley Geochronological Center Special Publication 1a.

McClelland, W.C. and Mattinson, J.M., 2000. Cretaceous-Tertiary evolution of the western Coast Mountains, central southeastern Alaska. *In:* Tectonics of the Coast Mountains in southeast Alaska and British Columbia, H.H. Stowell and W.C. McClelland (eds.), Geological Society of America, Special Paper 343, p. 159-182.

Mezger, J.E., 2000. 'Alpine-type' ultramafic rocks of the Kluane metamorphic assemblage, southwest Yukon: Oceanic crust fragments of a late Mesozoic back-arc basin along the northern coast Belt. *In:* Yukon Exploration and Geology 1999, D.S. Emond and L.H. Weston (eds.), Exploration and Geological Services Division, Yukon Region, Indian and Northern Affairs Canada, p. 127-138.

Mezger, J.E., Chacko, T. and Erdmer, P., 2001a. Metamorphism at a late Mesozoic accretionary margin: a study from the Coast Belt of the North American Cordillera. Journal of metamorphic Geology, vol. 19, p. 121-137.

Mezger, J.E., Creaser, R., Erdmer, P. and Johnson, S.E., 2001b. A Cretaceous back-arc basin in the Coast Belt of the northern Canadian Cordillera: evidence from geochemical and neodynium isotope characterisitics of the Kluane metamorphic assemblage, southwest Yukon. Canadian Journal of Earth Sciences, vol. 38, p. 91-103.

Miller, L.D., Stowell, H.H. and Gehrels, G.E., 2000. Progressive deformation associated with mid-Cretaceous to Tertiary contractional tectonism in the Juneau gold belt, Coast Mountains southeastern Alaska. *In:* Tectonics of the Coast Mountains, Southeastern Alaska and British Columbia, H.H. Stowell and W.C. McClelland (eds.), Geological Society of America, Special Paper 343, p. 193-233.

Miller, L.D., Goldfarb, R.J., Gehrels, G.E. and Snee, L.W., 1994. Genetic links among fluid cycling, vein formation, regional deformation and plutonism in the Juneau gold belt, southeastern Alaska. Geology, vol. 22, p. 203-206.

Miller, L.D., Goldfarb, R.J., Gent, C.A. and Kirkham, R.A., 1995. Structural geology, age, mechanisms of gold formation at the Kensington deposits, Berners Bay district, southeast Alaska. Economic Geology, vol. 90, p. 343-368.

Muller, J.E., 1967. Kluane Lake map-area, Yukon Territory. Geological Survey of Canada, Memoir 340, p. 137.

Murphy, D.C., 2007. The three 'Windy McKinley' terranes of Stevenson Ridge (115JK), western Yukon. *In:* Yukon Exploration and Geology, D.S. Emond, L.L. Lewis and L.H. Weston (eds.), Yukon Geological Survey, p. 223-236.

Murphy, D.C., van Staal, C.R. and Mortensen, J.K., 2008. Windy McKinley terrane, Stevenson Ridge area (115JK), western Yukon: composition and proposed correlations, with implications for mineral potential. *In:* Yukon Exploration and Geology, D.S. Emond, L.R. Blackburn, R.P. Hill and L.H. Weston (eds.), Yukon Geological Survey, p. 225-235.

Murphy, D.C., Mortensen, J.K. and van Staal, C.R., 2009. 'Windy-McKinley' terrane, western Yukon: new data bearing on its composition, age, correlation and paleotectonic settings. *In:* Yukon Exploration and Geology, L.H. Weston, L.R. Blackburn and L.L. Lewis (eds.), Yukon Geological Survey, p. 195-209.

Murphy, D.C., Mortensen, J.K., Piercey, S.J., Orchard, M.J. and Gehrels, G.E., 2006. Mid-Paleozoic to early Mesozoic tectonostratigraphic evolution of Yukon-Tanana and Slide Mountain terranes and affiliated overlap assemblages, Finlayson Lake massive sulphide district, southeastern Yukon. *In:* Paleozoic evolution and metallogeny of pericratonic terranes at the ancient Pacific margin of North America, Canadian and Alaskan Cordillera, M. Colpron and J.L. Nelson (eds.), Geological Association of Canada, Special Paper 45, p. 75-105.

Nelson, J.L., Colpron, M., Piercey, S.J., Dusel-Bacon, C., Murphy, D.C. and Roots, C.F., 2006. Paleozoic tectonic and metallogenic evolution of the pericratonic terranes in Yukon, northern British Columbia and eastern Alaska. *In:* Paleozoic evolution and metallogeny of pericratonic terranes at the ancient Pacific margin of North America, Canadian and Alaskan Cordillera, M. Colpron and J.L. Nelson (eds.), Geological Association of Canada, Special Paper 45, p. 323-360.

Piercey, S.J., Nelson, J.L., Colpron, M., Dusel-Bacon, C., Simard, R.-L. and Roots, C.F., 2006. Paleozoic magmatism and crustal recycling along the ancient Pacific margin of North America, northern Cordillera. *In:* Paleozoic evolution and metallogeny of pericratonic terranes at the ancient Pacific margin of North America, Canadian and Alaskan Cordillera, M. Colpron and J.L. Nelson (eds.), Geological Association of Canada, Special Paper 45, p. 281-322.

Smith, F.M., 1971. Geological and geochemical report on the Alaskite project claims Ed and Add groups, Claim sheet 115G8, Rockslide and Alaskite Ck area Yukon Territory. Yukon Territorial Assessment Report 060194, 33 p.

Tempelman-Kluit, D.J., 1974. Reconnaissance geology of Aishihik Lake, Snag and part of Stewart River map areas, west-central Yukon. Geological Survey of Canada, Paper 73-21.

Trigg, Woollett and Associates., 1971. Exploration 1971-Max Mineral Claim Group, Ryholite Creek, Yukon Territory. Yukon Territorial Mineral Assessment Report 060991, 90 p.

Wengzynowski, W., 1995. Prospecting, soil geochemistry, trenching and geophysical surveys at the Ruby Range project. Yukon Territorial Assessment Report 093250, 148 p.

Wheeler, J.O. and McFeely, P., 1991. Tectonic assemblage map of the Canadian Cordillera and adjacent parts of the United States of America. Geological Survey of Canada, scale 1:2 000 000.

Yukon MINFILE, 2009. Yukon MINFILE – A database of mineral occurrences. Yukon Geological Survey, <*http://www.geology.gov.yk.ca/databases_gis.html*>.

Appendix 1. *Detrital zircon data for sample 09SIT11*

	CONCORDIA COLUMNS							2 s %	2 s %	2 s %	AGES Ma						Concordia	2σ error	MSWD	Probability	ppm	ppm	Ratio
	207/235	7/5 err	206/238	6/8 err	Rho	207/206	7/6 err	207/235	206/238	207/206	7/5 age	1 sigma	6/8 age	1sigma	7/6 age	1 sigma	age (Ma)	Ma	(of concordance)		Th232	U238	Th/U
Phanerozoic Ages																							
no09a07	0.0998	0.0055	0.0129	0.0008	0.5920	0.0698	0.0081	10.9	13.0	23.2	97	5	83	5	922	238	90.4	9.2	8.76	0.003	15	34	0.42
no09a08	0.0985	0.0048	0.0151	0.0009	0.6237	0.0508	0.0033	9.7	12.1	12.9	95	4	96	6	233	149	95.6	8.7	0.06	0.809	25	68	0.36
no09a09	0.2469	0.0107	0.0307	0.0007	0.2812	0.0602	0.0027	8.7	4.9	9.0	224	9	195	5	611	97	198.5	9.1	11.26	0.001	82	220	0.37
no09a11	0.2014	0.0088	0.0298	0.0006	0.2292	0.0513	0.0027	8.8	4.0	10.6	186	7	189	4	255	122	188.7	7.2	0.14	0.706	66	135	0.49
no09a12	0.1734	0.0066	0.0243	0.0004	0.2228	0.0535	0.0024	7.6	3.4	8.8	162	6	155	3	352	100	155.4	5.1	1.84	0.175	271	558	0.49
no09a15	0.3875	0.0188	0.0524	0.0015	0.2848	0.0549	0.0024	9.7	5.5	8.8	333	14	329	9	407	98	330.0	16.7	0.05	0.822	61	126	0.48
no09a24	0.2169	0.0076	0.0318	0.0007	0.3184	0.0512	0.0023	7.0	4.5	9.1	199	6	202	4	252	105	201.1	8.3	0.14	0.713	66	252	0.26
no09a25	0.2198	0.0068	0.0318	0.0006	0.2989	0.0518	0.0019	6.2	3.7	7.2	202	6	202	4	278	83	201.6	6.9	0.00	0.974	96	253	0.38
no09a27	0.1201	0.0037	0.0185	0.0004	0.3697	0.0488	0.0020	6.2	4.6	8.0	115	3	118	3	138	94	117.0	4.8	0.61	0.436	95	331	0.29
no09a30	0.2175	0.0078	0.0313	0.0008	0.3752	0.0527	0.0023	7.2	5.4	8.8	200	7	199	5	316	100	199.1	9.6	0.03	0.866	35	114	0.31
no09a34	0.1035	0.0076	0.0149	0.0007	0.3133	0.0566	0.0069	14.6	9.2	24.2	100	7	95	4	476	268	96.0	8.2	0.51	0.476	45	73	0.61
no09a36	0.1886	0.0083	0.0279	0.0005	0.1910	0.0504	0.0021	8.8	3.4	8.2	175	7	177	3	213	95	177.3	5.7	0.08	0.783	114	278	0.41
no09a37	0.1907	0.0094	0.0282	0.0006	0.2274	0.0502	0.0023	9.8	4.5	9.3	177	8	179	4	203	108	179.0	7.6	0.07	0.798	168	338	0.50
no09a49	0.0990	0.0047	0.0151	0.0003	0.2450	0.0492	0.0028	9.5	4.6	11.2	96	4	97	2	158	131	96.5	4.3	0.03	0.863	317	688	0.46
no09a50	0.2283	0.0166	0.0330	0.0015	0.3068	0.0536	0.0042	14.5	8.9	15.6	209	14	209	9	356	177	209.1	17.1	0.00	0.974	43	91	0.48
no09a51	0.1334	0.0186	0.0198	0.0022	0.4043	0.0538	0.0096	27.9	22.6	35.7	127	17	126	14	363	403	126.7	25.4	0.00	0.965	37	81	0.46
no09a52	0.1882	0.0082	0.0294	0.0010	0.3888	0.0472	0.0020	8.7	6.8	8.5	175	7	187	6	58	101	182.1	10.9	2.67	0.102	197	489	0.40
no09a54	0.0990	0.0049	0.0148	0.0004	0.2472	0.0491	0.0023	9.9	4.9	9.2	96	5	95	2	153	108	94.9	4.4	0.06	0.806	353	662	0.53
no09a60	0.1805	0.0082	0.0247	0.0007	0.3158	0.0550	0.0030	9.0	5.7	11.0	169	7	157	4	411	123	159.3	8.4	2.65	0.104	79	303	0.26
no09a62	0.1040	0.0063	0.0135	0.0004	0.2482	0.0570	0.0032	12.0	6.0	11.1	100	6	87	3	491	123	87.9	5.0	5.81	0.016	191	291	0.65
no09a64	0.1100	0.0057	0.0153	0.0005	0.2961	0.0554	0.0041	10.4	6.2	14.9	106	5	98	3	428	166	99.3	5.8	2.33	0.127	113	238	0.47
no09a70	0.1167	0.0066	0.0152	0.0004	0.2248	0.0587	0.0039	11.3	5.1	13.5	112	6	97	2	555	147	98.2	4.8	6.23	0.013	137	222	0.62
no09a74	0.2717	0.0124	0.0349	0.0008	0.2522	0.0575	0.0025	9.1	4.6	8.5	244	10	221	5	510	94	224.1	9.7	5.17	0.023	54	154	0.35
no09a75	0.1027	0.0032	0.0151	0.0002	0.2533	0.0505	0.0017	6.2	3.2	6.7	99	3	97	2	218	77	97.0	2.9	0.76	0.384	116	395	0.29
no09a76	0.0964	0.0026	0.0149	0.0002	0.2307	0.0483	0.0016	5.5	2.5	6.7	93	2	95	1	112	79	94.8	2.3	0.41	0.522	351	1087	0.32
no09a86	0.4050	0.0091	0.0523	0.0007	0.2990	0.0567	0.0013	4.5	2.7	4.8	345	7	329	4	482	52	332.5	8.1	5.92	0.015	123	378	0.33
no09a88	0.0951	0.0031	0.0145	0.0002	0.2452	0.0488	0.0017	6.5	3.2	7.2	92	3	93	1	138	84	92.7	2.8	0.04	0.838	154	528	0.29
no09a95	0.1317	0.0118	0.0200	0.0009	0.2525	0.0491	0.0035	18.0	9.1	14.4	126	11	128	6	154	168	127.5	11.0	0.05	0.830	45	131	0.35
no09a98	0.0980	0.0042	0.0155	0.0003	0.2139	0.0472	0.0021	8.5	3.6	9.1	95	4	99	2	60	108	98.5	3.5	1.12	0.291	125	336	0.37
no09a100	0.4087	0.0301	0.0523	0.0017	0.2139	0.0576	0.0049	14.8	6.3	17.0	348	22	329	10	514	187	330.8	19.6	0.76	0.383	14	91	0.16
no09a101	0.2318	0.0111	0.0340	0.0008	0.2407	0.0501	0.0023	9.5	4.6	9.0	212	9	215	5	200	104	214.8	9.3	0.16	0.689	48	260	0.18
no09a107	0.3953	0.0173	0.0533	0.0012	0.2624	0.0547	0.0020	8.7	4.6	7.3	338	13	335	7	400	82	335.6	14.2	0.07	0.798	241	765	0.32
no09a109	0.1843	0.0071	0.0270	0.0005	0.2223	0.0503	0.0017	7.7	3.4	6.9	172	6	172	3	208	79	172.0	5.6	0.00	0.965	171	487	0.35
no09a112	0.1369	0.0064	0.0206	0.0005	0.2586	0.0498	0.0027	9.4	4.9	10.8	130	6	131	3	186	126	131.3	6.0	0.04	0.838	122	301	0.41
no09a113	0.0939	0.0040	0.0130	0.0004	0.3955	0.0566	0.0027	8.6	6.8	9.6	91	4	83	3	477	106	85.5	5.2	4.39	0.036	53	120	0.44
no09a119	0.2291	0.0065	0.0320	0.0005	0.2699	0.0534	0.0017	5.7	3.1	6.2	209	5	203	3	348	70	203.9	5.9	1.50	0.221	108	259	0.42
no09a120	0.0978	0.0042	0.0149	0.0005	0.3870	0.0531	0.0032	8.6	6.7	12.2	95	4	96	3	333	138	95.3	5.8	0.05	0.827	52	123	0.43
no09a121	0.2113	0.0100	0.0308	0.0008	0.2616	0.0522	0.0029	9.5	5.0	11.0	195	8	196	5	296	126	195.6	9.1	0.02	0.894	41	157	0.26
no09a122	0.1100	0.0057	0.0158	0.0005	0.2966	0.0520	0.0027	10.4	6.2	10.4	106	5	101	3	286	119	102.1	5.9	0.80	0.371	187	385	0.49
no09a123	0.2128	0.0119	0.0308	0.0009	0.2518	0.0527	0.0033	11.2	5.6	12.6	196	10	196	5	318	143	195.6	10.4	0.00	0.974	29	121	0.24
no09a126	0.4178	0.0129	0.0567	0.0008	0.2256	0.0544	0.0017	6.2	2.8	6.4	354	9	355	5	387	72	355.3	9.2	0.01	0.921	101	270	0.37
no09a130	0.2108	0.0071	0.0313	0.0005	0.2466	0.0506	0.0018	6.8	3.3	7.0	194	6	199	3	224	81	198.2	6.2	0.59	0.442	58	239	0.24
no09a131	0.0996	0.0052	0.0144	0.0004	0.2922	0.0532	0.0035	10.5	6.2	13.2	96	5	92	3	339	150	92.7	5.4	0.85	0.356	136	480	0.28
no09a132	0.2121	0.0084	0.0312	0.0007	0.2811	0.0510	0.0021	7.9	4.4	8.3	195	7	198	4	240	96	197.6	8.2	0.17	0.681	98	225	0.43
no09a133	0.2416	0.0050	0.0351	0.0003	0.2304	0.0513	0.0012	4.1	1.9	4.6	220	4	222	2	255	53	221.9	4.0	0.37	0.544	99	718	0.14
no09a137	0.2234	0.0066	0.0318	0.0006	0.3166	0.0530	0.0018	5.9	3.7	6.9	205	5	202	4	328	78	202.7	6.9	0.24	0.626	100	303	0.33
no09a138	0.1011	0.0042	0.0167	0.0004	0.2572	0.0449	0.0017	8.2	4.2	7.5	98	4	107	2	-63	91	105.1	4.3	5.35	0.021	43	680	0.06
no09a139	0.0955	0.0077	0.0154	0.0010	0.3861	0.0485	0.0047	16.0	12.4	19.5	93	7	98	6	124	230	96.1	10.8	0.59	0.442	51	142	0.36
no09a144	0.1034	0.0056	0.0149	0.0005	0.2880	0.0553	0.0040	10.9	6.3	14.6	100	5	95	3	422	163	96.2	5.7	0.73	0.393	46	119	0.39
no09a145	0.0875	0.0051	0.0142	0.0007	0.4191	0.0501	0.0039	11.7	9.8	15.7	85	5	91	4	199	182	88.5	7.7	1.48	0.224	33	85	0.38
no09a146	0.2031	0.0053	0.0292	0.0004	0.2580	0.0517	0.0015	5.2	2.7	5.9	188	4	185	2	271	67	185.8	4.7	0.25	0.614	184	497	0.37
no09a151	0.1076	0.0029	0.0168	0.0002	0.2471	0.0477	0.0014	5.4	2.7	5.9	104	3	108	1	83	70	107.0	2.7	2.02	0.156	452	842	0.54
no09a152	0.2623	0.0137	0.0324	0.0009	0.2658	0.0608	0.0037	10.4	5.5	12.2	237	11	205	6	630	131	209.0	10.9	7.91	0.005	24	104	0.23
no09a153	0.2118	0.0073	0.0312	0.0005	0.2164	0.0507	0.0018	6.9	3.0	7.1	195	6	198	3	225	83	197.9	5.7	0.29	0.593	116	383	0.30
no09a156	0.2114	0.0112	0.0309	0.0009	0.2800	0.0513	0.0028	10.6	5.9	10.9	195	9	196	6	256	125	195.8	10.8	0.02	0.892	63	234	0.27
no09a157	0.1046	0.0060	0.0156	0.0004	0.1988	0.0503	0.0031	11.4	4.5	12.2	101	5	100	2	209	142	100.1	4.4	0.03	0.857	98	400	0.24
no09a159	0.1663	0.0032	0.0243	0.0003	0.2929	0.0509	0.0011	3.8	2.2	4.3	156	3	155	2	238	50	155.0	3.2	0.29	0.588	483	1472	0.33
no09a160	0.0942	0.0052	0.0141	0.0004	0.2406	0.0498	0.0032	10.9	5.3	12.8	91	5	90	2	188	149	90.3	4.6	0.08	0.776	77	384	0.20
no09a161	0.0995	0.0053	0.0147	0.0004	0.2486	0.0501	0.0025	10.7	5.3	10.1	96	5	94	2	199	118	94.5	4.8	0.18	0.675	178	482	0.37
no09a162	0.2224	0.0069	0.0319	0.0004	0.1982	0.0515	0.0016	6.2	2.4	6.2	204	6	202	2	262	71	202.3	4.7	0.09	0.765	132	978	0.14
no09a163	0.1014	0.0051	0.0144	0.0006	0.3840	0.0529	0.0027	10.1	7.8	10.3	98	5	92	4	323	117	93.6	6.6	1.73	0.189	18	409	0.04
Precambrian Ages																							
no09a38	4.7953	0.0527	0.3185	0.0027	0.3808	0.1113	0.0011	2.2	1.7	2.0	1784	9	1782	13	1821	18	1783.7	17.4	0.02	0.891	82	184	0.45
no09a39	5.3082	0.1200	0.3354	0.0056	0.3678	0.1181	0.0032	4.5	3.3	5.5	1870	19	1865	27	1928	49	1868.8	36.2	0.04	0.836	29	34	0.85
no09a48	5.1197	0.0782	0.3282	0.0035	0.3512	0.1148	0.0017	3.1	2.1	2.9	1839	13	1830	17	1877	26	1836.5	23.8	0.30	0.587	83	144	0.58
no09a56	11.4497	0.1563	0.4888	0.0057	0.4275	0.1735	0.0026	2.7	2.3	3.0	2560	13	2566	25	2592	25	2560.8	25.4	0.05	0.818	30	57	0.53
no09a73	6.2866	0.0687	0.3577	0.0042	0.5312	0.1288	0.0016	2.2	2.3	2.6	2017	10	1971	20	2082	23	2017.9	19.1	7.41	0.006	130	233	0.56
no09a83	1.8404	0.0508	0.1813	0.0026	0.2570	0.0746	0.0021	5.5	2.8	5.7	1060	18	1074	14	1058	57	1069.2	24.7	0.48	0.487	48	180	0.27
no09a85	5.5991	0.1407	0.3439	0.0070	0.4069	0.1193	0.0022	5.0	4.1	3.8	1916	22	1905	34	1946	34	1914.2	42.0	0.11	0.740	120	145	0.83
no09a148	6.9175	0.1411	0.3487	0.0052	0.3660	0.1463	0.0022	4.1	3.0	3.0	2101	18	1929	25	2303	26	2048.6	34.8	48.12	0.000	111	190	0.58
no09a149	3.3930	0.1105	0.2215	0.0052	0.3581	0.1127	0.0019	6.5	4.7	3.4	1503	26	1290	27	1844	31	1389.4	45.5	48.53	0.000	123	207	0.59

Appendix 2. *Detrital zircon data for sample 08DM126.*

Analysis No.	$^{207}Pb/^{235}U$ Ma	$^{207}Pb/^{235}U$ +/- 1σ Error	$^{206}Pb/^{238}U$ Ma	$^{206}Pb/^{238}U$ +/- 1σ Error	$^{207}Pb/^{206}Pb$ Ma	$^{207}Pb/^{206}Pb$ +/- 1σ Error	Preferred Age Ma *	Preferred Age +/- 1σ Error	Discordancy %
08DM-126L2	104.2	2.16	104.5	1.01	112.5	53.27	**104.5**	**1.0**	7.1
08DM-126L3	83.1	22.65	83.1	4.54	89.1	565.96	**83.1**	**4.5**	6.7
08DM-126L4	80	0.96	79.7	0.69	85.9	35.03	**79.7**	**0.7**	7.2
08DM-126L5	195	3.55	191.4	1.86	211.7	46.72	**191.4**	**1.9**	9.6
08DM-126L6	86	3.62	81.7	1.26	199	100.8	**81.7**	**1.3**	58.9
08DM-126L7	79.6	3.7	79.5	1.14	77.5	113.42	**79.5**	**1.1**	-2.6
08DM-126L8	191.4	2.93	190.6	1.75	199.6	40.61	**190.6**	**1.8**	4.5
08DM-126L9	87.4	4.26	87.4	1.35	85.5	118.87	**87.4**	**1.4**	-2.2
08DM-126L10	112	1.76	111.7	1.05	109.3	41.95	**111.7**	**1.1**	-2.2
08DM-126L11	193.3	3.02	191.5	1.8	191.4	41.13	**191.5**	**1.8**	-0.1
08DM-126L12	88	5.26	88.1	1.61	88.4	143.95	**88.1**	**1.6**	0.3
08DM-126L13	167.4	5.63	166.1	2.08	180.1	82.27	**166.1**	**2.1**	7.8
08DM-126L15	78.2	4.19	78	1.18	75.7	129.55	**78.0**	**1.2**	-3.0
08DM-126L16	80	2.01	80.4	0.86	85.8	64.32	**80.4**	**0.9**	6.3
08DM-126L17	328.1	3.64	328.3	2.87	335.4	31.07	**328.3**	**2.9**	2.1
08DM-126L18	180.2	2.33	180.5	1.63	180.5	35.49	**180.5**	**1.6**	0.0
08DM-126L19	207	4.85	199.4	2.31	201.9	57.58	**199.4**	**2.3**	1.2
08DM-126L20	101	1.58	101.2	0.96	102.1	41.58	**101.2**	**1.0**	0.9
08DM-126L21	108.2	4.29	112.4	1.83	131.9	96.11	**112.4**	**1.8**	14.8
08DM-126L22	105.1	7.33	79.7	2.06	797.6	149.09	**79.7**	**2.1**	90.0
08DM-126L23	117.3	2.58	116	1.27	130.8	55.65	**116.0**	**1.3**	11.3
08DM-126L24	187.5	3.11	185.1	1.83	186.1	42.97	**185.1**	**1.8**	0.5
08DM-126L25	95.2	2.73	94.4	1.08	92.4	72.46	**94.4**	**1.1**	-2.2
08DM-126L26	126.8	3.93	128.5	1.56	122.8	76.79	**128.5**	**1.6**	-4.6
08DM-126L27	197.2	2.69	195	1.86	201	36.26	**195.0**	**1.9**	3.0
08DM-126L28	91.1	2.41	87.3	1.1	103.5	66	**87.3**	**1.1**	15.7
08DM-126L29	187.9	2.05	185.8	1.68	205.4	30.62	**185.8**	**1.7**	9.5
08DM-126L30	295.4	3.61	294.5	2.72	301.2	33.06	**294.5**	**2.7**	2.2
08DM-126L31	78.8	3.26	78.6	1.12	79.9	101.53	**78.6**	**1.1**	1.6
08DM-126L32	1823.2	22.18	1807	16.74	1835.4	27.22	**1835.4**	**27.2**	1.5
08DM-126L33	146.1	11.83	148.2	3.64	164.3	188.99	**148.2**	**3.6**	9.8
08DM-126L34	97.3	4.67	96.6	1.59	107.9	115.69	**96.6**	**1.6**	10.5
08DM-126L35	81.1	1.76	79.7	0.88	77.6	55.74	**79.7**	**0.9**	-2.7
08DM-126L36	1822.7	10.25	1819.4	14.53	1813.5	20.95	**1813.5**	**21.0**	-0.3
08DM-126L37	106.2	1.13	105.9	0.97	120.1	29.65	**105.9**	**1.0**	11.8
08DM-126L38	85.6	4.34	84.6	1.36	86.4	123.32	**84.6**	**1.4**	2.1
08DM-126L39	213.1	13.72	207.6	4.91	215.7	149.79	**207.6**	**4.9**	3.8
08DM-126L40	206.9	8.9	205.8	3.58	204.3	101.89	**205.8**	**3.6**	-0.7
08DM-126L41	1168.1	13.18	1142.9	10.67	1251.2	28.42	**1251.2**	**28.4**	8.7
08DM-126L42	82	3.21	83.2	1.32	85.5	96.34	**83.2**	**1.3**	2.7
08DM-126L43	83.7	6.82	83.8	2.01	92.6	192.37	**83.8**	**2.0**	9.5
08DM-126L44	173.6	6.08	171.6	2.56	174.6	84.52	**171.6**	**2.6**	1.7
08DM-126L45	197.4	6.11	192.8	2.62	189.7	75.18	**192.8**	**2.6**	-1.6
08DM-126L46	194.4	3.92	192.8	2.18	194.5	50.01	**192.8**	**2.2**	0.9
08DM-126L47	103.5	3.02	101.3	1.39	111.8	71.62	**101.3**	**1.4**	9.4
08DM-126L48	342.4	3.68	341.1	3.22	337.2	29.3	**341.1**	**3.2**	-1.2
08DM-126L49	195	7.12	198.1	3.02	205.8	87.67	**198.1**	**3.0**	3.7
08DM-126L50	121.6	3.39	119.5	1.46	125.3	68.57	**119.5**	**1.5**	4.6
08DM-126L51	207.6	5.04	205.6	2.64	218.9	59.85	**205.6**	**2.6**	5.6
08DM-126L52	170.4	5.14	174.5	2.49	172.6	74.03	**174.5**	**2.5**	0.1
08DM-126L53	82.8	9.76	82.6	2.02	80.3	270.69	**82.6**	**2.0**	-3.0
08DM-126L54	104.9	6.86	105.9	2.46	100.5	156.48	**105.9**	**2.5**	-4.9
08DM-126L55	206.8	6.53	208.3	2.95	200.5	77.44	**208.3**	**3.0**	-3.5
08DM-126L56	110.8	1.78	110.1	1.22	112.6	40.93	**110.1**	**1.2**	1.9
08DM-126L57	77.8	2.79	77.5	1.23	81.7	88.94	**77.5**	**1.2**	5.0
08DM-126L58	82.6	1.49	82.4	0.94	87.7	46.4	**82.4**	**0.9**	5.9
08DM-126L59	188.9	3.91	189.4	2.28	190.7	51.48	**189.4**	**2.3**	0.8
08DM-126L60	114.8	5.29	103.2	1.72	382.8	106.66	**103.2**	**1.7**	71.5
08DM-126L61	170.5	6.14	173.6	2.71	183.1	87.41	**173.6**	**2.7**	6.0
08DM-126L62	79.9	3.41	80.3	1.27	87	104.68	**80.3**	**1.3**	7.9
08DM-126L63	81.8	9.05	82	2.35	92.2	255.9	**82.0**	**2.4**	11.2
08DM-126L64	76.9	3.73	78.2	1.38	77.7	118.23	**78.2**	**1.4**	0.2
08DM-126L65	83.4	2.61	84	1.24	83.4	77.87	**84.0**	**1.2**	-0.4